

Article

Africa's oldest dinosaurs reveal early suppression of dinosaur distribution

<https://doi.org/10.1038/s41586-022-05133-x>

Received: 10 September 2021

Accepted: 21 July 2022

Published online: 31 August 2022

 Check for updates

Christopher T. Griffin^{1,2,3}✉, Brenen M. Wynd¹, Darlington Munyikwa^{4,5}, Tim J. Broderick⁶, Michel Zondo⁵, Stephen Tolan⁷, Max C. Langer⁸, Sterling J. Nesbitt¹ & Hazel R. Taruringa^{5,9}

The vertebrate lineages that would shape Mesozoic and Cenozoic terrestrial ecosystems originated across Triassic Pangaea^{1–11}. By the Late Triassic (Carnian stage, ~235 million years ago), cosmopolitan ‘disaster faunas’ (refs. ^{12–14}) had given way to highly endemic assemblages^{12,13} on the supercontinent. Testing the tempo and mode of the establishment of this endemism is challenging—there were few geographic barriers to dispersal across Pangaea during the Late Triassic. Instead, palaeolatitudinal climate belts, and not continental boundaries, are proposed to have controlled distribution^{15–18}. During this time of high endemism, dinosaurs began to disperse and thus offer an opportunity to test the timing and drivers of this biogeographic pattern. Increased sampling can test this prediction: if dinosaurs initially dispersed under palaeolatitudinal-driven endemism, then an assemblage similar to those of South America^{4,19–21} and India^{19,22}—including the earliest dinosaurs—should be present in Carnian deposits in south-central Africa. Here we report a new Carnian assemblage from Zimbabwe that includes Africa’s oldest definitive dinosaurs, including a nearly complete skeleton of the sauropodomorph *Mbiresaurus raathi* gen. et sp. nov. This assemblage resembles other dinosaur-bearing Carnian assemblages, suggesting that a similar vertebrate fauna ranged high-latitude austral Pangaea. The distribution of the first dinosaurs is correlated with palaeolatitude-linked climatic barriers, and dinosaurian dispersal to the rest of the supercontinent was delayed until these barriers relaxed, suggesting that climatic controls influenced the initial composition of the terrestrial faunas that persist to this day.

In the wake of the end-Permian mass extinction, biogeography across the supercontinent Pangaea was largely uniform, with cosmopolitan taxa dispersed globally^{12–14}. As the Triassic progressed, ecosystems stabilized and recovered¹³ and endemism gradually increased¹² until, by the earliest part of the Late Triassic (Carnian stage, ~235 million years ago (Ma)), terrestrial faunas were largely segregated into distinct biogeographic provinces^{12,15–18}. Climatic regionalization resulting from a hothouse climate, strong seasonality and high atmospheric partial pressure of CO₂ (p_{CO_2}) created strong arid and humid palaeolatitudinal climate belts arranged from pole to pole across the supercontinent^{17,18,23} (Fig. 1a). These climatic regions have been proposed to have acted as effective obstacles to biogeographic dispersal, contributing to the endemism of Carnian faunas^{15–18}. Although this hypothesis was initially based on data from eastern North America¹⁷, recent work has suggested that this may have been a global driver of first-order biogeography during the Late Triassic^{16,18,24}.

This time of global endemism hosts the oldest definitive dinosaurs, but their record in the Carnian is both sparse and geographically limited²⁵. The earliest and best preserved dinosaurs are known exclusively from a few localities in central South America, within the Ischigualasto

Formation of northern Argentina^{4,20,21} and the Santa Maria Formation of southern Brazil^{4,26}. Most other early dinosaur records are far younger (~10–15 Ma; for example, the Chinle Formation²⁷) or only represented by loosely associated or isolated bones (lower Maleri Formation, central India^{22,28}). If dinosaur dispersal followed the broader patterns of faunal endemism during the Late Triassic, a similar faunal assemblage—including early dinosaurs—can be predicted to be present in Carnian-aged sediments of south-central Africa, which fill the palaeolatitudinal gap between modern-day central South America and India (Fig. 1).

Here we report a rich new fossil assemblage from the Carnian of Zimbabwe containing Africa’s oldest known dinosaurs—about equivalent in age to the oldest dinosaurs known anywhere—which greatly enhances knowledge of the origin and early evolution of the group across Pangaea. In addition to a nearly complete skeleton of a new taxon of sauropodomorph, this assemblage includes the remains of herrerasaurid dinosaurs, hyperodapedontine rhynchosauroids, gomphodontosuchine cynodonts, early-diverging aetosaurs and a possible dicynodont, revealing a palaeoecological assemblage strikingly similar to those of dinosaur-bearing Carnian stratigraphic units along this same palaeolatitude in South America and India^{4,20–22,26,28}.

¹Department of Geosciences, Virginia Tech, Blacksburg, VA, USA. ²Department of Earth and Planetary Sciences, Yale University, New Haven, CT, USA. ³Yale Peabody Museum of Natural History, Yale University, New Haven, CT, USA. ⁴National Museums and Monuments of Zimbabwe, Harare, Zimbabwe. ⁵Department of Geology and Paleontology, Natural History Museum of Zimbabwe, Bulawayo, Zimbabwe. ⁶Makari, Chisipite, Harare, Zimbabwe. ⁷Chipembere Wildlife Education Centre, Mfuwe, Zambia. ⁸Departamento de Biología, Universidade de São Paulo, São Paulo, Brazil.

⁹School of Agriculture and Natural Sciences, Great Zimbabwe University, Masvingo, Zimbabwe. [✉]e-mail: chris.griffin@yale.edu

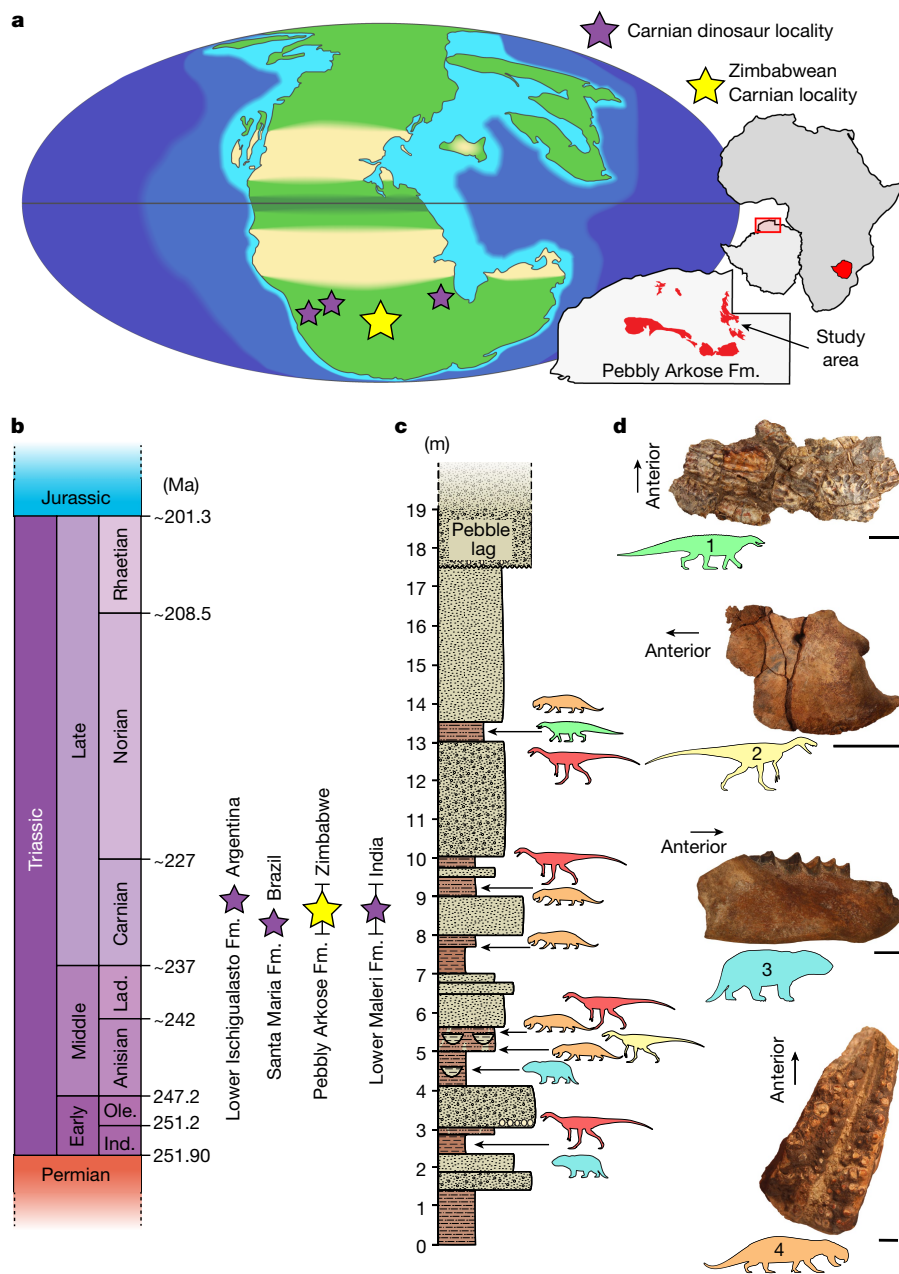


Fig. 1 | The new Zimbabwean assemblage is on the same palaeolatitudinal climatic belt as other Carnian dinosaur-bearing assemblages and has a similar taxonomic composition. **a**, The northern Zimbabwean locality geographically links other Carnian dinosaurian localities across southern Pangaea. **b**, The new Zimbabwean locality is the oldest definitive dinosaurian locality in Africa, coeval with Carnian dinosaur localities from other parts of the world. Ind., Indian; Ole., Olenekian. **c**, Summary stratigraphic column of the Pebby Arkose Formation at the type locality in Zimbabwe showing the

records of *Mbiresaurus raathi* gen. et sp. nov (red), a herrerasaurid dinosaur (yellow), a traversodontid cynodont (blue), a hyperodapedontine rhynchosaur (orange) and an aetosaur (green). **d**, Representative fossils from the Pebby Arkose Formation, including (1) aetosaur paramedian osteoderm (dorsal view), (2) herrerasaurid dinosaur coracoid (lateral view), (3) cynodont dentary (lateral view) and (4) hyperodapedontine rhynchosaur maxilla (occlusal view). Scale bars: 1 cm (fossils 1, 3 and 4) and 5 cm (fossil 2). Climatic belts follow ref.¹⁸.

Systematic Palaeontology

Dinosauria Owen, 1842

Saurischia Seeley, 1887

Sauropodomorpha von Huene, 1932

Mbiresaurus raathi gen. et sp. nov.

Etymology. From *Mbire*, an historic Shona empire and district containing the study area, and *σαῦρος* (*sauros*), Greek for reptile; *raathi* after Michael

Raath, who with others first reported fossils from the Dande area²⁹, to honour his contribution to Zimbabwean palaeontology and the fossil heritage of Zimbabwe.

Holotype. NHMZ (Natural History Museum of Zimbabwe, Bulawayo, Zimbabwe) 2222, a nearly complete, associated and partially articulated skeleton including a partial cranium, cervical, trunk, sacral and caudal vertebrae, rib fragments, partial pectoral and pelvic girdles, and partial forelimbs and hindlimbs.

Referred material. NHMZ 2547, larger partial skeleton found with holotype.

Locality and horizon. From the midsection of the ?late Carnian Pebbley Arkose Formation^{30,31}, Dande Communal Land, Mbire District, Mashonaland Central Province, Zimbabwe (Extended Data Figs. 1 and 2). Coordinates for specific localities are available on request through C.T.G. and NHMZ. See the Supplementary Information for detailed justification of formation age.

Diagnosis. *Mbiresaurus raathi* differs from all other sauropodomorphs in the following combination of character states: frontal more than twice as anteroposteriorly long as mediolaterally wide; dorsal margin of the anterior portion of the dentary deflected ventrally; orbital margin of the postorbital projects into the orbit; postorbital fits into a slot in the frontal; slightly recurved dentary teeth with mesial and distal carinae and small denticles; at least 20 maxillary teeth; sacrum composed of three sacral vertebrae with a dorsosacral vertebra and two primordial sacral vertebrae; deltopectoral crest extends anteriorly at an angle of ~90° from the long axis of the humeral head in proximal view; width of the distal end of the humerus less than one-third the proximodistal length of the element; supra-acetabular crest of the ilium extends approximately two-thirds down (distal) the lateral side of the pubic peduncle; slightly concave ventral border of the iliac acetabular wall; anteroposteriorly short and dorsoventrally broad postacetabular process of the ilium with well-developed brevis shelf (autapomorphy); long axis of the femoral head almost parallel to the distal intercondylar line; olecranon process remains not fused to the ulna late in ontogeny (potential autapomorphy, evidence for ontogenetic variability) (Fig. 2 and Extended Data Fig. 9; see the Supplementary Information for extended differential diagnosis).

Ontogenetic assessment. Histology of the tibia of NHMZ 2222 indicates that longitudinal growth had slowed but had not ceased (Extended Data Fig. 3). Prominent bone scars in its fore- and hindlimb are strongly suggestive of morphological maturity in early dinosaurs^{32–34}. The scapula is not fused to the coracoid (often uninformative of maturity³²), and the olecranon is not fused to the ulna (probably autapomorphic for this taxon). The neurocentral sutures of the vertebrae are all closed. Although NHMZ 2222 had not completely ceased growth (that is, was skeletally immature³⁴), it attained most features indicative of morphological maturity. The paratype (NHMZ 2547) is ~15% larger than NHMZ 2222, indicating that either size increased after morphological maturity or there was variation in the maximum body size of individuals, as in other early dinosaurs^{32–34}.

Description

The ventral border of the premaxilla of *Mbiresaurus raathi* is at the same horizontal level as that of the maxilla (Fig. 2). As in later sauropodomorphs^{35,36} and *Bagualosaurus*³⁷, but unlike in most Carnian sauropodomorphs, *M. raathi* lacks a subnarial gap. There is a premaxillary foramen on the anteroventral margin of the narial fossa (Fig. 2x), a feature that has been recovered as a synapomorphy of both *Eusaurischia*³⁸ and *Ornithoscelida*³⁹. The ventral margin of the antorbital fossa on the maxilla is marked by a sharp ridge (Fig. 2w), as in most Carnian sauropodomorphs and early neotheropods, but unlike the more rounded feature of *Eoraptor*⁴⁰. The frontal pair of *M. raathi* is anteroposteriorly longer than it is mediolaterally wide, unlike in most Carnian sauropodomorphs, but similar to later members of the group (for example, *Plateosaurus*, *Adeopapposaurus* and *Massospondylus*). The most anterior portion of the dorsal surface of the dentary is deflected ventrally (Fig. 2r), a likely sauropodomorph synapomorphy²⁶, although this is clearer in *Bagualosaurus* and later sauropodomorphs (M.C.L., personal observation). There are denticles on both the mesial and distal margins of the premaxillary teeth in *M. raathi*, as in later sauropodomorphs (for example, *Plateosaurus*³⁵) but unlike in many Carnian sauropodomorphs from South America such as *Eoraptor*, *Pampadromaeus* and *Buriolestes*²⁶, although some (for example, *Pampadromaeus* and *Bagualosaurus*) completely lack serration in some premaxillary teeth^{37,41}.

The dentary teeth are arranged *en échelon* and are labiolingually compressed and slightly recurved. Both mesial and distal carinae possess apically oriented denticles along their lengths (Fig. 2r,s), forming the imbricated ‘leaf-shaped’ teeth typical of early sauropodomorphs⁴². The denticles are relatively small (seven denticles per millimetre; Fig. 2s) compared with those of some early sauropodomorphs such as *Pampadromaeus* and *Bagualosaurus*²⁶.

The cervical centra are twice as anteroposteriorly long as they are dorsoventrally tall and lack pneumatic fossae (Fig. 2c), as in *Eoraptor* and other early sauropodomorphs⁴³. The trunk vertebrae of *M. raathi* possess hypophene–hypsanthrum accessory articulations, a saurischian synapomorphy⁴⁴. The sacrum is composed of three vertebrae (Fig. 2a), with a dorsosacral vertebra added anterior to the primordial two sacral vertebrae, as in some Carnian^{43,45} and most later³⁶ sauropodomorphs, early ornithischians (*Eocursor*, *Heterodontosaurus* and *Lesothosaurus*) and neotheropods⁴⁰, but unlike in other Carnian sauropodomorphs, which possess an additional sacral vertebra incorporated from the caudal series^{26,46}. Unlike in other Carnian sauropodomorphs⁴⁷, but as in later-diverging taxa⁴⁷, the sacral centra of the paratype (NHMZ 2548) are co-ossified, although those of the smaller holotype (NHMZ 2222) are not.

The distal end of the scapular blade is ~2.5 times wider than the proximal ‘neck’ of the blade (Fig. 2q), as in other Carnian sauropodomorphs (*Saturnalia* and *Eoraptor*) and unlike the strap-shaped blade of herrerasaurids⁴⁸. As in other early sauropodomorphs²⁶, the deltopectoral crest of the humerus is long and asymmetric, and its apex extends to ~40% the length of the humerus (Fig. 2p). The deltopectoral crest of the humerus is more anteriorly directed than in many other Carnian sauropodomorphs^{43,49} but is similar to that in *Guaibasaurus*⁵⁰, *Pampadromaeus*⁴¹ and later sauropodomorphs⁵¹. The olecranon process is not fused to the ulna in the type and referred specimens of *M. raathi*, and there is a rounded, rugose ‘biceps tubercle’ (as in *Saturnalia*⁴⁹) integrated into the anterior side of the proximal end of the ulna (Fig. 2n).

The ilium of *M. raathi* is robustly built, with thick, large and well-integrated bone scars across the blade (Fig. 2b). As in other early sauropodomorphs, but unlike in herrerasaurids and early theropods⁴⁵, the acetabulum is anteroposteriorly shorter than it is dorsoventrally tall. The ventral edge of the iliac acetabular wall is slightly concave, forming a ‘perforate’ acetabulum (Fig. 2b) that is a classic dinosaurian synapomorphy⁴⁰, similar to the acetabular wall in later sauropodomorphs³⁶ and different from the ventrally straight acetabular walls in several other Carnian sauropodomorphs²⁶. The ilium of *M. raathi* possesses an autapomorphic posterior process that is ‘robust’ (anteroposteriorly short and dorsoventrally broad), similar to the ilia of later sauropodomorphs, but with a well-developed brevis shelf (Fig. 2b and Extended Data Fig. 10). The distal end of the ischium has a distal expansion (Fig. 2l) similar in form to that of early sauropodomorphs but unlike that of *Herrerasaurus*⁴⁶.

The femur is sigmoidal in shape, with a curved shaft and an anteromedially directed head with an offset anteromedial tuber, a dinosaurian synapomorphy⁴⁰. The bone scars of the femur (for example, the anterolateral trochanter, trochanteric shelf and intermuscular lines) are distinct, large and robust (Fig. 2g), similar to those of *Herrerasaurus*⁵² and mature individuals of *Coelophysoides*³². Variation in femoral bone scars of *M. raathi* (Extended Data Fig. 9), and within *Saturnalia*, suggests that these scars are ontogenetically variable as in other Triassic dinosauriforms³³. The distal margin of the fourth trochanter of the femur is sharply angled (~90°) towards the femoral shaft (Extended Data Fig. 9), as in most other early sauropodomorphs^{26,43,46} and *Herrerasaurus*⁵². The fibular condyle is much larger than the lateral condyle (= crista tibiofibularis), and these are separated by a clear groove. The tibia is the same length as the femur, and its cnemial crest is well developed and anterolaterally directed (Fig. 2f), similar to that of many early dinosaurs²⁶. As in some herrerasaurids and Carnian sauropodomorphs,

Article

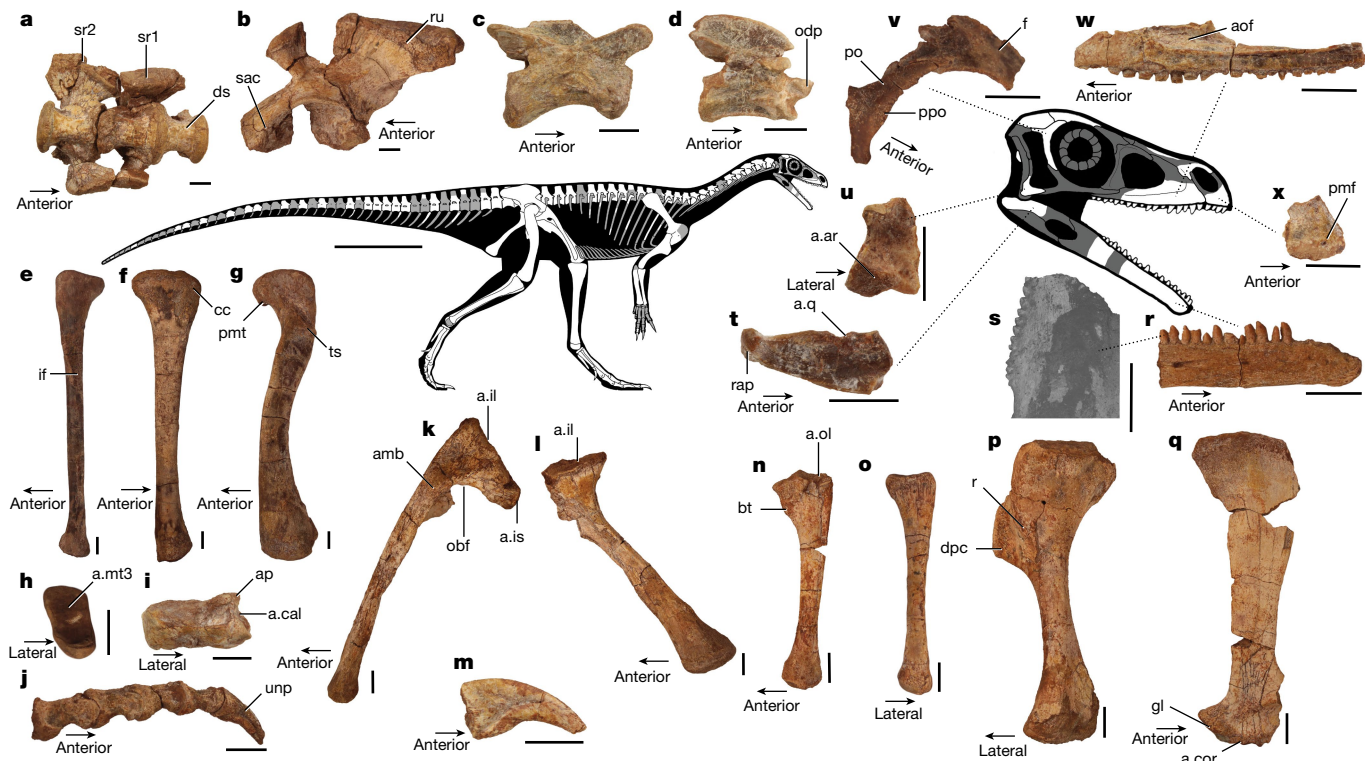


Fig. 2 | Skeletal anatomy of the *Mbiresaurus raathi* holotype (NHMZ 2222) and paratype (NHMZ 2547). **a**, Sacrum (NHMZ 2547). **b**, Left ilium (NHMZ 2547). **c**, Cervical vertebra (NHMZ 2547). **d**, Axis (NHMZ 2547). **e**, Left fibula (NHMZ 2222). **f**, Left tibia (NHMZ 2222). **g**, Left femur (NHMZ 2222). **h**, Right tarsal III (NHMZ 2222). **i**, Right astragalus (NHMZ 2222). **j**, Left pedal phalanges (NHMZ 2222). **k**, Left pubis (NHMZ 2547). **l**, Left ischium (NHMZ 2547). **m**, Manual ungual (NHMZ 2222). **n**, Left ulna (NHMZ 2222). **o**, Right radius (NHMZ 2547). **p**, Left humerus (NHMZ 2222). **q**, Right scapula (NHMZ 2547). **r**, Right dentary (NHMZ 2222). **s**, Scanning electron microscope image of dentary tooth. **t**, Right articular and surangular (NHMZ 2222). **u**, Left quadrate (NHMZ 2222). **v**, Right frontal and postorbital (NHMZ 2222). **w**, Left maxilla (NHMZ 2222). **x**, Right premaxilla (NHMZ 2222). Orientations: **a**, ventral; **b–h**, **j–n**, **q–t**, **w**, **x**, lateral; **f**, **j**, medial; **g**, anterolateral; **h**, distal;

i, **o**, posterior; **p**, posterolateral; **u**, anterior; **v**, posterodorsal. Scale bars: 1 cm (**a–r**, **t**–**x**), 1 mm (**s**) and 20 cm (skeletal reconstruction). Grey elements are unknown. *a.*, articulates with; *amb.*, ambiens process; *aof.*, antorbital fossa; *ap.*, ascending process; *ar.*, articular; *bt.*, biceps tubercle; *cal.*, calcaneum; *cc.*, cnemial crest; *cor.*, coracoid; *dpc.*, deltopectoral crest; *ds.*, dorsosacral vertebra; *f.*, frontal; *gl.*, glenoid; *if.*, musculus iliofibularis attachment scar; *il.*, ilium; *is.*, ischium; *mt3.*, metatarsal III; *obf.*, obturator foramen; *odp.*, odontoid process; *ol.*, olecranon; *pmf.*, premaxillary foramen; *pmt.*, posteromedial tuber; *po.*, postorbital; *ppo.*, postorbital projection into orbit; *q.*, quadrate; *r.*, ridge; *rap.*, retroarticular process; *ru.*, rugosity; *sac.*, supra-acetabular crest; *srl.*, sacral rib; *prim.*, primordial sacral 1; *sr2.*, sacral rib, primordial sacral 2; *ts.*, trochanteric shelf; *unp.*, pedal ungual.

but unlike in early theropods (for example, *Tawa*, GR 242), the distal end of the tibia is roughly quadrangular in distal view. As in most early dinosaurs⁴⁰, the third metatarsal is the longest (Extended Data Fig. 9). The pedal unguals are less recurved than in herrerasaurids and theropods, and their ventral surface is flat, similar to those of other early sauropodomorphs (for example, *Eoraptor*⁴³ and *Saturnalia*⁴⁶).

Analyses and discussion

Because the phylogeny of early dinosaurs and their kin is currently controversial, we tested the phylogenetic affinities of *M. raathi* with several recently published character matrices^{26,39,53} using maximum parsimony, as well as with a Bayesian approach (Fig. 3a and Extended Data Fig. 4). *M. raathi* was consistently recovered among the earliest diverging sauropodomorphs (Fig. 3a and Extended Data Fig. 4). In the parsimony analyses, it was recovered in a similar position or forming a clade of Carnian sauropodomorphs, or in a polytomy at the base of Saurischia with other Carnian sauropodomorphs (Extended Data Fig. 4). Thus, these results are independent evidence that *M. raathi* is an early sauropodomorph, anatomically similar to Carnian-aged members of the group from the same palaeolatitude of southern Pangaea.

The rest of the assemblage recovered from the Pebby Arkose Formation of the Dande Communal Area is similar in taxonomic composition

to assemblages from the terrestrial Carnian sediments of Argentina, Brazil and India, matching the biogeographic prediction given by the similar palaeolatitudinal position of these regions. A hyperodapedontine rhynchosaur (*Hyperodapedon* sp.) is the most common taxon (Fig. 1c and Extended Data Fig. 5), strongly suggesting a temporal correlation with the Carnian *Hyperodapedon* Assemblage Zone of Brazil⁴ and the *Hyperodapedon*–*Exaeretodon*–*Herrerasaurus* biozone of Argentina^{20,21,54}. Supporting this idea, the Pebby Arkose assemblage also hosts an *Exaeretodon*-like cynodont, an *Aetosauroides*-like aetosaur and a large (~6-m-long) early-diverging saurischian dinosaur (Extended Data Fig. 5), all low-level clades that have been recovered from the Ischigualasto Formation of Argentina^{20,21}, the Santa Maria Formation of Brazil^{4,19} and the lower Maleri Formation of India^{19,22,28}. This distinctive assemblage of taxa found alongside the earliest known dinosaurs strongly suggests a common faunal setting for the earliest dinosaurs. These assemblages are found along the same palaeolatitudinal zone (Fig. 1a), indicating that these taxa may be tracking latitudinally controlled climate belts, which have been proposed to have been a major influence on tetrapod distribution across Late Triassic Pangaea^{15–18}.

Triassic dinosaurs in particular have been proposed to have been biogeographically restricted by these climate belts, with sauropodomorphs restricted to higher latitudes with greater humidity and

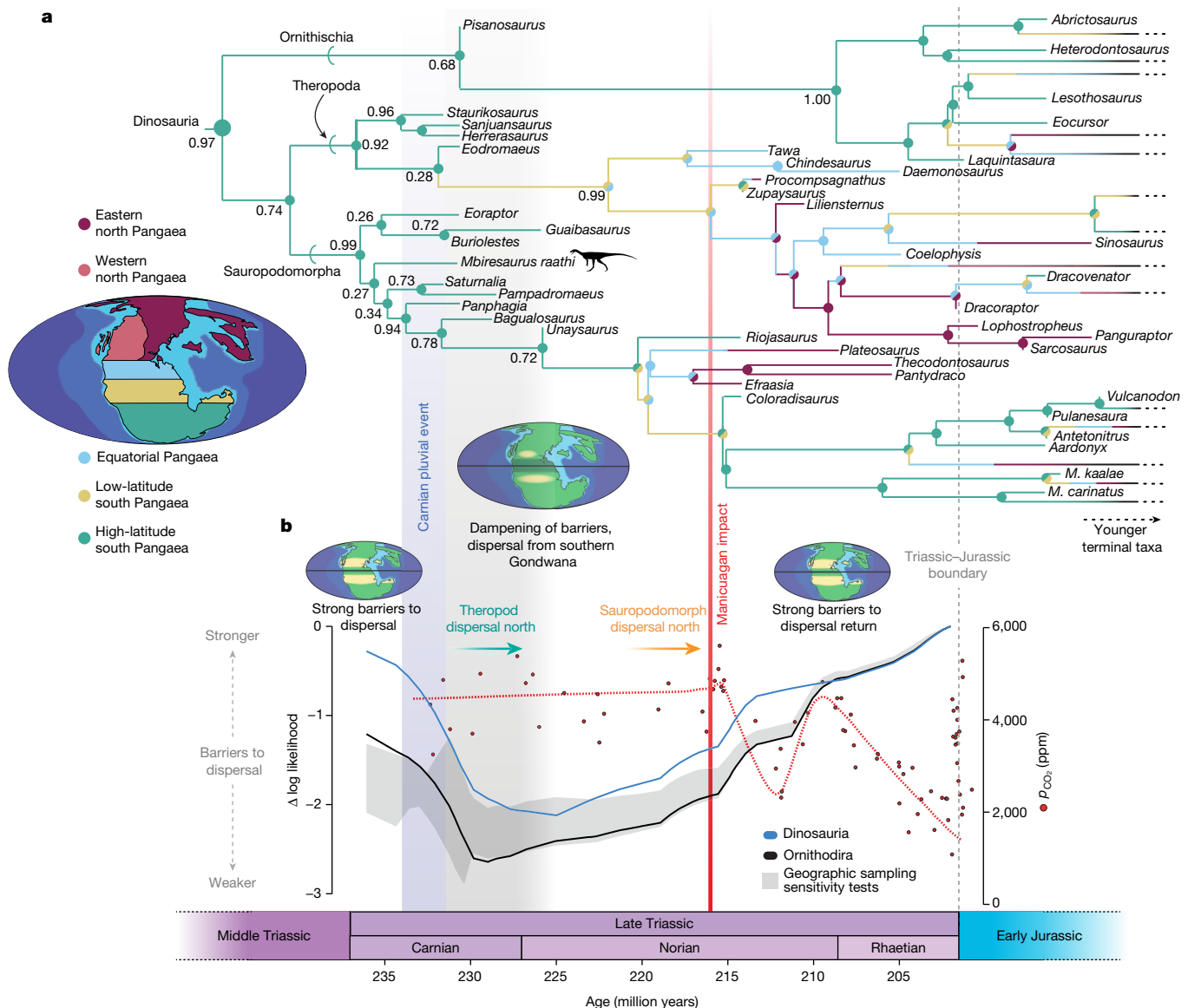


Fig. 3 | The tempo and mode of Triassic dinosaur dispersal. **a**, Phylogenetic relationships of early dinosaurs, with *Mbiresaurus raathi* recovered as an early sauropodomorph. The ancestral geographic range of early dinosaurs was high-latitude southern Pangaea, with theropods dispersing north in the late Carnian, followed by sauropodomorphs in the Norian. *M. kaalae*, *Massospondylus kaalae*; *M. carinatus*, *Massospondylus carinatus*. **b**, The biogeographic dispersal model suggests a higher likelihood of climatic barriers to dispersal from southern Pangaea early in dinosaurian and

ornithodiran evolution, with barriers dampened in the late Carnian and early Norian before returning for the remainder of the Triassic. P_{CO_2} proxy data are from ref. ⁶⁰. The phylogeny is from the Bayesian analysis of the modified dataset in ref. ⁵³ (Methods); numbers at early nodes indicate posterior probabilities to two significant digits. Posterior probabilities for all nodes are given in Extended Data Fig. 6. Early nodes were given no a priori time constraint; deep divergences (for example, Dinosauria, Saurischia, Theropoda and Sauropodomorpha) may be slightly younger than estimated by the model.

more abundant vegetation^{16,18}. Conversely, although early theropods have been considered to be more climatically resilient¹⁶, the more arid and unstable low latitudes are thought to have promoted a delay in dinosaurian numerical abundance worldwide throughout the Late Triassic^{16,18}. We tested this hypothesis of climatic barriers to dinosaurian dispersal by exploring whether the early phylogenetic history of dinosaurs retains a signal for restricted dispersal. We implemented a dispersal-extinction-cladogenesis (DEC) model⁵⁵ on our tip-dated phylogeny under a maximum-likelihood framework. We generated different rate matrices of biogeographic dispersal across Pangaea, estimating pre-arid belt, arid belt and post-Triassic dispersal. The date of the arid belt dispersal matrix was tested along the entire Late Triassic, with the difference in likelihood (delta-likelihood) indicating whether this dispersal pattern was supported at any given time; that

is, a lower likelihood indicates dispersal across arid belts, suggesting decreased strength of climatic barriers. Therefore, the model used the ornithodiran phylogeny to estimate when, if ever, there were barriers to dinosaurian dispersal from high-latitude southern Pangaea during the Late Triassic.

Our model recovered a tripartite pattern indicating that early dinosaurian dispersal was influenced by a waxing and waning of climatic barriers (Fig. 3b). Although there is support for barriers to dinosaurian dispersal at the earliest stage of their evolution, by 230 Ma these barriers had broken down. This sharp dip in barrier delta-likelihood is roughly coincident with the Carnian pluvial event, a global period of extended humidity that would be expected to lessen the intensity of tropical arid belts. This initial breakdown was followed by ~5–7 million years of modelled dispersal of dinosaurs to northern palaeolatitudes. Following this,

Article

the model suggests less dispersal across climatic zones for the remainder of the Triassic, which is interpreted here as a re-establishment of climatic barriers and a predominance of endemic cladogenesis. An exception to this trend is a steep uptick in delta-likelihood at ~215 Ma, coincident with the Manicouagan impact, and a subsequent plateau (or even decline; Extended Data Fig. 7) during the following global decrease in atmospheric p_{CO_2} that has been independently proposed to have encouraged dispersal northwards by sufficiently removing climatic barriers²⁸. Including non-dinosaurian ornithodirans in the model resulted in the same general pattern of dispersal, and our sensitivity analyses recovered similar trends of restriction–dispersal–restriction, suggesting that this signal is not driven by incomplete sampling of northern Carnian assemblages or phylogenetic uncertainty (Fig. 3b and Extended Data Figs. 6 and 7). Combined with the ancestral state estimation (Fig. 3a), our model suggests that the early evolution of dinosaurs was marked by biogeographic constraint to the higher latitudes of southern Pangea, with two waves of northward colonization: first theropods, in the latest portion of the Carnian, followed by sauropodomorphs in the Norian. The constraints on dispersal then returned for the remainder of the Triassic, mooring taxa in their respective biogeographic provinces across Pangaea. We therefore predict that any late Carnian dinosaurs recovered outside this southern temperate belt will be theropods. An independent, preliminary report of a late Carnian–early Norian theropod from Wyoming⁵⁶ supports our hypothesis of theropod-first dispersal, but increased sampling from 220–215 Ma will provide further tests of this model.

The Triassic—especially the Late Triassic—was the cradle of lineages that went on to shape the terrestrial vertebrate communities of the Mesozoic and Cenozoic, including mammals¹⁷, turtles^{5,6}, lissamphibians^{8,10}, lepidosaurs^{3,9,11}, crocodylomorphs² and, of course, the dinosaurs and their kin⁴. The biogeographic context of the early evolution of these lineages has received much attention^{57–59}, but sparse sampling has often obscured the earliest history of major groups, including dinosaurs. Our detailed hypothesis of how latitudinal climate belts influenced dispersal across Pangaea has clear implications for the terrestrial biogeography of the Late Triassic: the distribution of dinosaurs suggests a waxing and waning of climatic barriers to dispersal across different regions of Pangaea. These barriers could have influenced the early dispersal of clades in different ways, still retaining the same global signal; for example, theropods and sauropodomorphs were both affected by the same climatic barriers, but the tempo and mode of their dispersal differed according to their reconstructed ecologies^{16,18}. This not only provides a broad framework for interpreting biogeography across the Triassic, but also can guide targeted, hypothesis-based fieldwork to new localities. Phylogenetic history may retain signals of abiotic disruption and its resulting influence on dispersal, and models of biogeography similar to what we have constructed for dinosaurs may offer productive avenues for uncovering the early history and assemblage of Mesozoic terrestrial vertebrate faunas.

Online content

Any methods, additional references, Nature Research reporting summaries, source data, extended data, supplementary information, acknowledgements, peer review information; details of author contributions and competing interests; and statements of data and code availability are available at <https://doi.org/10.1038/s41586-022-05133-x>.

- Debuyschere, M., Gheerbrant, E. & Allain, R. Earliest known European mammals: a review of the Morganucodonta from Saint-Nicolas-de-Port (Upper Triassic, France). *J. Syst. Palaeontol.* **13**, 825–855 (2015).
- Irmis, R., Nesbitt, S. J. & Sues, H.-D. In *Anatomy, Phylogeny and Palaeobiology of Early Archosaurs and Their Kin* Vol. 239 (eds Nesbitt, S. J. et al.) 275–302 (2013).
- Jones, M. E. H. et al. Integration of molecules and new fossils supports a Triassic origin for Lepidosauria (lizards, snakes, and tuatara). *BMC Evol. Biol.* **13**, 208 (2013).
- Langer, M. C., Ramezani, J. & Da Rosa, Á. A. S. U-Pb age constraints on dinosaur rise from south Brazil. *Gondwana Res.* **57**, 133–140 (2018).
- Li, C., Wu, X.-C., Rieppel, O., Wang, L.-T. & Zhao, L.-J. An ancestral turtle from the Late Triassic of southwestern China. *Nature* **456**, 497–501 (2008).
- Lyson, T. R. & Bever, G. S. Origin and evolution of the turtle body plan. *Ann. Rev. Ecol. Evol. Syst.* **51**, 143–166 (2020).
- Mao, F., Zhang, C., Liu, C. & Meng, J. Fossiloriality and evolutionary development in two Cretaceous mammaliamorphs. *Nature* **592**, 577–582 (2021).
- Schoch, R. R., Werneburg, R. & Voigt, S. A Triassic stem-salamander from Kyrgyzstan and the origin of salamanders. *Proc. Natl Acad. Sci. USA* **117**, 11584–11588 (2020).
- Simões, T. R. et al. The origin of squamates revealed by a Middle Triassic lizard from the Italian Alps. *Nature* **557**, 706–709 (2018).
- Stocker, M. R. et al. The earliest equatorial record of frogs from the Late Triassic of Arizona. *Biol. Lett.* **15**, 20180922 (2019).
- Martinez, R. N., Simões, T. R., Sobral, G. & Apesteguía, S. A Triassic stem lepidosaur illuminates the origin of lizard-like reptiles. *Nature* **597**, 235–238 (2021).
- Button, D. J., Lloyd, G. T., Ezcurra, M. D. & Butler, R. J. Mass extinctions drove increased global faunal cosmopolitanism on the supercontinent Pangaea. *Nat. Commun.* **8**, 733 (2017).
- Chen, Z.-Q. & Benton, M. J. The timing and pattern of biotic recovery following the end-Permian mass extinction. *Nat. Geosci.* **5**, 375–383 (2012).
- Roopnarine, P. D., Angielczyk, K. D., Wang, S. C. & Hertog, R. Trophic network models explain instability of Early Triassic terrestrial communities. *Proc. Biol. Sci.* **274**, 2077–2086 (2007).
- Ezcurra, M. D. Biogeography of Triassic tetrapods: evidence for provincialism and driven sympatric cladogenesis in the early evolution of modern tetrapod lineages. *Proc. R. Soc. B* **277**, 2547–2552 (2010).
- Kent, D. V. & Clemmensen, L. B. Northward dispersal of dinosaurs from Gondwana to Greenland at the mid-Norian (215–212 Ma, Late Triassic) dip in atmospheric pCO_2 . *Proc. Natl Acad. Sci. USA* **118**, e2020778118 (2021).
- Whiteside, J. H., Grogan, D. S., Olsen, P. E. & Kent, D. V. Climatically driven biogeographic provinces of Late Triassic tropical Pangaea. *Proc. Natl Acad. Sci. USA* **108**, 8972–8977 (2011).
- Whiteside, J. H. et al. Extreme ecosystem instability suppressed tropical dinosaur dominance for 30 million years. *Proc. Natl Acad. Sci. USA* **112**, 7909–7913 (2015).
- Langer, M. C. Studies on continental Late Triassic tetrapod biochronology. II. The Ischigualastian and a Carnian global correlation. *J. South Amer. Earth Sci.* **19**, 219–239 (2005).
- Martinez, R. N. et al. Vertebrate succession in the Ischigualasto Formation. *J. Vertebr. Paleontol.* **32**, 10–30 (2012).
- Colombi, C. et al. A high-precision U–Pb zircon age constraints the timing of the faunistic and palynofloristic events of the Carnian Ischigualasto Formation, San Juan, Argentina. *J. South Amer. Earth Sci.* **111**, 103433 (2021).
- Novas, F. E., Ezcurra, M. D., Chatterjee, S. & Kutty, T. S. New dinosaur species from the Upper Triassic Upper Maleri and Lower Dharmaram formations of Central India. *Earth Environ. Sci. Trans. R. Soc. Edin.* **101**, 333–349 (2010).
- Sellwood, B. W. & Valdes, P. J. Mesozoic climates: general circulation models and the rock record. *Sediment. Geol.* **190**, 269–287 (2006).
- Kligrman, B. T., Marsh, A. D., Sues, H.-D. & Sidor, C. A. A new non-mammalian eucynodont from the Chinle Formation (Triassic: Norian), and implications for the early Mesozoic equatorial cynodont record. *Biol. Lett.* **16**, 20200631 (2020).
- Irmis, R. B. Evaluating hypotheses for the early diversification of dinosaurs. *Earth Environ. Sci. Trans. R. Soc. Edin.* **101**, 397–426 (2010).
- Cabreira, S. F. et al. A unique Late Triassic dinosauromorph assemblage reveals dinosaur ancestral anatomy and diet. *Curr. Biol.* **26**, 3090–3095 (2016).
- Irmis, R. B., Mundil, R., Martz, J. W. & Parker, W. G. High-resolution U–Pb ages from the Upper Triassic Chinle Formation (New Mexico, USA) support a diachronous rise of dinosaurs. *Earth Planet. Sci. Lett.* **309**, 258–267 (2011).
- Langer, M. C., Ezcurra, M. D., Bittencourt, J. S. & Novas, F. E. The origin and early evolution of dinosaurs. *Biol. Rev.* **85**, 55–110 (2010).
- Raath, M. A., Oesterlen, P. M. & Kitching, J. W. First record of Triassic Rhynchosauria (Reptilia: Diapsida) from the Lower Zambezi Valley, Zimbabwe. *Palaeontologia Africana* **29**, 1–10 (1992).
- Oesterlen, P. M. The geology of the Dande West Area, Lower Zambezi Valley. *Zimbabwe Geol. Soc. Bull.* **98**, 1–85 (1998).
- Sciscio, L. et al. Sedimentology and palaeontology of the Upper Karoo Group in the Mid-Zambezi Basin, Zimbabwe: new localities and their implications for interbasinal correlation. *Geol. Mag.* **158**, 1035–1058 (2021).
- Griffin, C. T. Developmental patterns and variation among early theropods. *J. Anat.* **232**, 604–640 (2018).
- Griffin, C. T. & Nesbitt, S. J. Anomalously high variation in postnatal development is ancestral for dinosaurs but lost in birds. *Proc. Natl Acad. Sci. USA* **113**, 14757–14762 (2016).
- Griffin, C. T. et al. Assessing ontogenetic maturity in extinct saurian reptiles. *Biol. Rev.* **96**, 470–525 (2021).
- Prieto-Márquez, A. & Norell, M. A. Redescription of a nearly complete skull of *Plateosaurus* (Dinosauria: Sauropodomorpha) from the Late Triassic of Trossingen (Germany). In *American Museum Novitates* 1–58 (American Museum of Natural History, 2011).
- Yates, A. M. The species taxonomy of the sauropodomorph dinosaurs from the Löwenstein Formation (Norian, Late Triassic) of Germany. *Palaeontology* **46**, 317–337 (2003).
- Pretto, F. A., Langer, M. C. & Schultz, C. L. A new dinosaur (Saurischia: Sauropodomorpha) from the Late Triassic of Brazil provides insights on the evolution of sauropodomorph body plan. *Zool. J. Linnean Soc.* **185**, 388–416 (2018).
- Ezcurra, M. D. A new early dinosaur (Saurischia: Sauropodomorpha) from the Late Triassic of Argentina: a reassessment of dinosaur origin and phylogeny. *J. Syst. Palaeontol.* **8**, 371–425 (2010).
- Baron, M. G., Norman, D. B. & Barrett, P. M. A new hypothesis of dinosaur relationships and early dinosaur evolution. *Nature* **543**, 501–506 (2017).

40. Nesbitt, S. J. The early evolution of archosaurs: relationships and the origin of major clades. in *Bulletin of the American Museum Natural History* 1–292 (American Museum of Natural History, 2011).
41. Langer, M. C., McPhee, B. W., Marsola, J. C. D. A., Roberto-da-Silva, L. & Cabreira, S. F. Anatomy of the dinosaur *Pampadromaeus barberenai* (Saurischia—Saurodromorpha) from the Late Triassic Santa Maria Formation of southern Brazil. *PLoS ONE* **14**, e0212543 (2019).
42. Martinez, R. N. & Alcober, O. A. A basal saurodromorpha (Dinosauria: Saurischia) from the Ischigualasto Formation (Triassic, Carnian) and the early evolution of Saurodromorpha. *PLoS ONE* **4**, e4397 (2009).
43. Sereno, P. C., Martinez, R. N. & Alcober, O. A. Osteology of *Eoraptor lunensis* (Dinosauria, Saurodromorpha). *J. Vertebr. Paleontol.* **32**, 83–179 (2012).
44. Stefanic, C. M. & Nesbitt, S. J. The evolution and role of the hypophene–hypantrum articulation in Archosauria: phylogeny, size and/or mechanics? *R. Soc. Open Sci.* **6**, 190258 (2019).
45. Marsola, J. C. A. et al. A new dinosaur with theropod affinities from the Late Triassic Santa Maria Formation, south Brazil. *J. Vertebr. Paleontol.* **38**, e1531878 (2019).
46. Langer, M. C. The pelvic and hind limb anatomy of the stem-saurodromorpha *Saturnalia tupiniquim* (Late Triassic, Brazil). *PaleoBios* **23**, 1–30 (2003).
47. Moro, D., Kerber, L., Müller, R. T. & Pretto, F. A. Sacral co-ossification in dinosaurs: the oldest record of fused sacral vertebrae in Dinosauria and the diversity of sacral co-ossification patterns in the group. *J. Anat.* **238**, 828–844 (2021).
48. Sereno, P. C. The pectoral girdle and forelimb of the basal theropod *Herrerasaurus ischigualastensis*. *J. Vertebr. Paleontol.* **13**, 425–450 (1994).
49. Langer, M. C., França, M. A. G. & Gabriel, S. The pectoral girdle and forelimb anatomy of the stem-saurodromorpha *Saturnalia tupiniquim* (Upper Triassic, Brazil). *Spec. Papers Palaeontol.* **77**, 113–137 (2007).
50. Langer, M. C., Bittencourt, J. S. & Schultz, C. L. A reassessment of the basal dinosaur *Guaibasaurus candelariensis*, from the Late Triassic Caturrita Formation of south Brazil. *Earth Environ. Sci. Trans. R. Soc. Edin.* **101**, 301–332 (2010).
51. Yates, A. M. A new species of the primitive dinosaur *Thecodontosaurus* (Saurischia: Saurodromorpha) and its implications for the systematics of early dinosaurs. *J. Syst. Paleontol.* **1**, 1–42 (2003).
52. Novas, F. E. New information on the systematics and postcranial skeleton of *Herrerasaurus ischigualastensis* (Theropoda: Herrerasauridae) from the Ischigualasto Formation (Upper Triassic) of Argentina. *J. Vertebr. Paleontol.* **13**, 400–423 (1994).
53. Langer, M. C. et al. Untangling the dinosaur family tree. *Nature* **551**, E1–E3 (2017).
54. Desojo, J. B. et al. The Late Triassic Ischigualasto Formation at Cerro Las Lajas (La Rioja, Argentina): fossil tetrapods, high-resolution chronostratigraphy, and faunal correlations. *Sci. Rep.* **10**, 12782 (2020).
55. Ree, R. H. & Smith, S. A. Maximum likelihood inference of geographic range evolution by dispersal, local extinction, and cladogenesis. *Syst. Biol.* **57**, 4–14 (2008).
56. Fitch, A. J., Lovelace, D. M. & Stocker, M. R. The oldest dinosaur from the northern hemisphere and the origins of Theropoda. in *Program and Abstracts 80th Annual Meeting of the Society of Vertebrate Paleontology* 140–141 (2020).
57. Evans, S. E. At the feet of the dinosaurs: the early history and radiation of lizards. *Biol. Rev.* **78**, 513–551 (2003).
58. Huttenlocker, A. K., Grossnickle, D. M., Kirkland, J. I., Schultz, J. A. & Luo, Z.-X. Late-surviving stem mammal links the lowermost Cretaceous of North America and Gondwana. *Nature* **558**, 108–112 (2018).
59. Lee, M. S. Y., Baron, M. G., Norman, D. B. & Barrett, P. M. Dynamic biogeographic models and dinosaur origins. *Earth Environ. Sci. Trans. R. Soc. Edin.* **109**, 325–332 (2018).
60. Schaller, M. F., Wright, J. D. & Kent, D. V. A 30 Myr record of Late Triassic atmospheric $p\text{CO}_2$ variation reflects a fundamental control of the carbon cycle by changes in continental weathering. *GSA Bull.* **127**, 661–671 (2015).

Publisher's note Springer Nature remains neutral with regard to jurisdictional claims in published maps and institutional affiliations.

Springer Nature or its licensor holds exclusive rights to this article under a publishing agreement with the author(s) or other rightsholder(s); author self-archiving of the accepted manuscript version of this article is solely governed by the terms of such publishing agreement and applicable law.

© The Author(s), under exclusive licence to Springer Nature Limited 2022

Article

Methods

This article was reviewed in English. The authors prepared summary statements written in Ndebele and Shona (which were not peer-reviewed or checked for correctness by Springer Nature) and have made them available at the online repository Dryad (<https://doi.org/10.5061/dryad.pg4f4qrqd>).

Fieldwork and preparation

All foreign researchers involved in fieldwork (C.T.G., S.T., S.J.N.) were registered with the Research Council of Zimbabwe for 2017 and 2019 field seasons (permit numbers 02991 and 03266 to C.T.G.; 02992 to S.T.; 03267 to S.J.N.). In the field, specimens were glued with Butvar-72 dissolved in acetone, which was removed during preparation with acetone. Fossils were first cleaned with water and toothbrushes before more intensive preparation with a Paleotools Microjack 1 under a dissection microscope. During preparation, clean breaks were glued with cyanoacrylate glue. We moulded elements with Smooth-On Mold Star 15 SLOW platinum silicone rubber and casted with Smooth-On Smooth Cast 300 liquid plastic resin.

Histological sampling

We histologically sampled the right tibia of the *Mbiresaurus raathi* holotype (NHMZ 2222) at midshaft (Extended Data Fig. 3), near where the element was already broken. To preserve the original morphology of the specimen, before sampling we moulded (using Smooth-On Mold Star 15 SLOW platinum silicone rubber) and casted (using Smooth-On Smooth Cast 300 liquid plastic resin) the tibia. We embedded the sample in Castolite AC clear polyester resin (Eager Polymers) and immediately placed this under vacuum for 2–3 min to remove bubbles. After curing, cross-sectional wafers were cut from the embedded specimen using an IsoMet 1000 precision diamond-bladed saw, with a wafer thickness of 1.5 mm. We polished one side of the wafer with progressively finer gridding discs (1,200 grit, 2,400 grit and a 0.3-µm polishing slurry) before gluing it with cyanoacrylate glue, polished side down, to a plexiglass microscope slide that had been roughened with sandpaper. The unpolished side of the wafer, facing up from the slide, was then, using the same method, ground and polished to a thickness that permitted the passage of enough light that histological structures were clear. We examined the slides with an Olympus BX51 petrographic microscope under three light regimes: plane-polarized light, cross-polarized light and cross-polarized light with a lambda retarder (530-nm gypsum wedge) to better observe the orientations of hydroxyapatite crystallites (which are in turn influenced by the orientation of the original collagen fibrils). We captured microscopy images with an Infinity1 camera and associated software. The large, whole-slide image was assembled from individual microscopy photographs using the Photomerge function in Adobe Photoshop v.22.3.0.

U–Pb detrital zircon dating

Zircons were disaggregated from a sandstone sample recovered from directly beneath the *Mbiresaurus raathi* holotype by Zirchron using conventional crushing and separation procedures. The Arizona Laserchron Center conducted U–Pb detrital zircon dating. The sample ($n = 300$) was mounted on a 1-inch epoxy mount, polished to a 1-µm finish and imaged with a Hitachi 3400N scanning electron microscope with backscatter. The laser ablation system was a Photon Machines Analyte G2 Excimer laser. Inductively coupled plasma mass spectrometry (ICP-MS) was conducted with a Thermo Element2 HR ICP-MS instrument.

Phylogenetic analyses

To robustly test the phylogenetic placement of *Mbiresaurus raathi*, we used three different matrices that sample the origins of major dinosaurian clades (from Cabreira et al.²⁶, Baron et al.³⁹ (as modified and expanded by others^{61–63}) and Langer et al.⁵³). Two of these matrices

sample the same characters, but differ in the character scores for many taxa^{39,53,61–63}). For these matrices, we added *Bagualosaurus agudoensis* along with *M. raathi*, but we only added *M. raathi* to the matrix from ref.²⁶. We also removed three controversial taxa: *Saltopus elginensis*, *Nyasasaurus parringtoni* and *Agnosphitys cromhallensis*. The *Agnosphitys* holotype is a chimera (personal observation, S.J.N.), and because *Saltopus* is known only from a mould⁶⁴ there are difficulties in scoring it consistently, with many character scores not unambiguously reproducible. *Nyasasaurus* is possibly a chimera⁶⁵ if all of the holotype and referred material is scored together (personal observation, S.J.N.), as has been done in these matrices, and, if only the highly incomplete holotype is scored, its position is very unstable and destroys most dinosauriform resolution. However, we also conducted analyses with these taxa to evaluate how they influenced the placement of *M. raathi*, confirming that they did not impact our interpretation of *Mbiresaurus* as an early sauropodomorph, for a total of six different phylogenetic analyses using parsimony (Extended Data Fig. 4). We followed ref.⁶⁶ in considering '*Marasuchus*' and junior synonym of *Lagosuchus*. Following ref.³⁹, we treated the following characters as ordered in the matrices from Baron et al.^{39,61–63} and Langer et al.⁵³: 24, 35, 29, 60, 68, 71, 117, 145, 167, 174, 180, 197, 199, 206, 214, 215, 222, 251, 269, 272, 286, 289, 303, 305, 307, 313, 322, 333, 334, 338, 353, 360, 376, 378, 393, 442 and 446. We removed character 217, which evaluates the co-ossification of sacral centra, because this character is highly variable in dinosaurian ontogeny^{32,34,47} and character states are probably related to the maturity of each individual scored more than to their phylogenetic relationships. For the matrix from Cabreira et al.²⁶, we treated the following characters as ordered, following ref.²⁶: 3, 4, 6, 11, 36, 60, 62, 64, 83, 115, 123, 139, 147, 148, 157, 160, 171, 173, 174, 178, 179, 182, 195, 200, 201, 202, 205, 216, 222, 240 and 248. We also rescored three character states in three taxa in this matrix that were binary but scored as multistate characters (*Heterodontosaurus* character 14: 2>0; *Dilophosaurus* character 86: 2>1; *Asilisaurus* character 223: 2>0). All trees were generated using equally weighted parsimony with TNT 1.5 (ref.⁶⁷), using Mesquite (v. 3.7)⁶⁸ to convert NEXUS files into *.tnt format. For each of the six analyses, a maximum of 99,999 trees were retained in memory, and a new technology search was performed using the sectorial searches, Ratchet and Tree Fusing algorithms with default settings. We searched for the most parsimonious tree until this tree was found 100 times (as in ref.⁵³) and retained resultant trees in memory. Following the new technology search, we performed a traditional search on the trees stored in memory using the tree bisection and reconnection search heuristic. To calculate reduced consensus trees, we found rogue taxa for each analysis (excluding *Mbiresaurus*, if necessary) using the command PCRPRUNE⁶⁹ in TNT, placing the resulting taxa in a taxon group. We then calculated the strict consensus tree while excluding this group of taxa, creating the reduced strict consensus tree.

Maximum likelihood has been suggested to better estimate phylogenetic relationships among extinct taxa from morphological characters⁷⁰ than the more conventional parsimony analyses, although this has been much debated^{71–74}. The latter approach has been more commonly used to investigate the controversial phylogeny of early ornithodirans^{26,39,40,53,75,76} (but see ref.⁷⁷). Bayesian inference of phylogenetic relationships, an expansion of the maximum-likelihood approach, has likewise been suggested to outperform parsimony analyses⁷⁸; specifically, a fossilized birth–death model has been suggested in simulations to better approximate true phylogenetic relationships among taxa known only from fossils than maximum parsimony⁷⁹. In light of this ongoing debate, we also used a Bayesian approach in analysing the modified matrix from Langer et al.⁵³ to both test the relationships of early dinosaurs further than with only our parsimony analyses (Extended Data Fig. 4) and generate phylogenetic trees appropriate for our biogeographic analyses. We generated a tip-dated phylogeny under Bayesian inference using Beast 2 (version 2.6.3)⁸⁰. We used the morph-models and sampled ancestors packages to analyse morphological matrices under a

fossilized birth–death model. We generated six distinct character partitions: two-state, three-state, three-state ordered, four-state, four-state ordered and six-state partitions. Beast 2 is not readily equipped to partition characters as ordered or unordered, and, as such, we manually coded the ordered character partitions by using rate matrices that force stepwise transitions between character states. We structured each of our six character partitions under an MK model with rates modelled under a gamma distribution with four different rate categories and a random local clock model set to 1.0 (ref. ⁸¹). For tip dates, we updated the dates used in ref. ⁵⁹ and included dates for our additional taxa, calculating tip dates as the mean age for the units in which each taxon occurs, based on radiometric and/or stratigraphic correlations (for a full list of dates and references, see Supplementary Table 3). We ran a Markov chain Monte Carlo (MCMC) model using the fossilized birth–death prior and forced monophyletic Archosauria and Ornithodira to set *Euparkeria capensis* and *Postosuchus kirkpatricki* as outgroup taxa. Otherwise, we used the default priors in Beaufit 2. We set the MCMC to run for 40,000,000 generations with a 50% pre-burn-in and to log a tree every 2,000 generations and ran 10 separate chains for a total of 210,010 sampled trees. We evaluated the output of the ten separate chains of our MCMC using Tracer⁸², with a 10% burn-in. Once we established convergence and sampling in our posterior sample of trees, we integrated the ten separate chains in LogCombiner by implementing a 10% burn-in on each separate chain, and, to avoid computational limitations, we resampled each chain to log a tree every 4,000 generations, for a final sample of 90,010 sampled trees. This was used to generate our maximum clade credibility tree with TreeAnnotator, with node heights set to the target heights of the tree and a 0% burn-in⁸³. We conducted this same procedure for the matrices from Baron et al.^{39,61,62} and Cabreira et al.²⁶ as well as for the matrix from Langer et al.⁵³ including the dinosauriform *Saltopus*, resulting in a total of four time-calibrated Bayesian maximum clade credibility trees (Fig. 3 and Extended Data Figs. 5 and 6). Note that these matrices were selected for their broad taxonomic sampling; interpretations of within-clade relationships, especially those of neotheropods and non-Carnian sauropodomorphs, should be taken with care.

Biogeographic dispersal model

Previous studies have focused on the biogeographic origins of Dinosauria⁵⁹, yet fewer studies have evaluated how biogeographic models can inform the timing of geographic or otherwise non-biological events^{84,85}. We aimed to test the origin of a major climatic event that limited dispersal across Pangea, given the biogeographic history and phylogeny of Dinosauria. Biogeographic analyses were performed in the R statistical environment (v.4.0.2)⁸⁶. We generated a DEC model under a maximum-likelihood framework, using the BioGeoBEARS package (v.1.1.2)^{87,88}, with three different dispersal rate matrices over the Triassic and Jurassic history of Ornithodira. We opted to use a single model, as we were testing the influence of limited dispersal across subtropical Pangaea, rather than estimating the most likely historical biogeography for Ornithodira. We therefore selected a DEC model because this is the simplest model that focuses on dispersal as the primary mode of colonization, using time-dependent probabilistic parameters, which is well suited for the data taken from the Triassic ornithodiran record⁸⁹. Our model must include parameters that force dispersal between adjacent areas, such that our model assumes that any dispersal event must have included an intermediate step, where the lineage was known from two locations simultaneously, making extinction of the home range occur before full colonization of the new range, rather than range expansion (dispersal) and home range extinction occurring simultaneously as is the case in the +J parameter⁸⁹ (Supplementary Information). Additionally, in testing how altering the origin of a climatic band affects model performance, only a model under which parameters are estimated using time-dependent probabilistic models would suffice—this is best captured by DEC. We therefore selected the DEC model to test our hypothesis for the timing of Triassic

dinosaurian dispersals. See the Supplementary Information for further justification for this model selection strategy.

We used three dispersal matrices to capture the early history of Ornithodira, the origin of a climatic belt that limited dispersal across Pangaea^{17,18} and the breakup of northern Pangaea in the earliest Jurassic (Extended Data Fig. 8). We set no a priori date for the origin of the arid climatic belt, and, as such, we used the ornithodiran phylogeny to estimate the timing of onset of this belt. We sampled five different geographic areas: high-latitude southern Pangaea, low-latitude southern Pangaea, equatorial Pangaea, western north Pangaea and eastern north Pangaea. We chose these areas because they reflect the presence of the arid belt (low-latitude southern Pangaea) and reflect the breakup of western and eastern north Pangaea (that is, the opening of the Hispanic Corridor and Viking Strait) at the beginning of the Jurassic^{90,91}. We built our model to randomly sample dates from a uniform distribution that spanned 235–201.5 Ma. For this interval, we used a dispersal rate matrix that limited dispersal from high-latitude to low-latitude southern Pangaea (probability = 0.5) and further limited dispersal from low-latitude southern Pangaea to equatorial Pangaea (probability = 0.25) and from high-latitude southern Pangaea to eastern and western north Pangaea (probability = 0.1). For the other two matrices, we used dispersal rates that limited dispersal from high-latitude southern Pangaea to equatorial Pangaea (probability = 0.5) or to eastern and western north Pangaea (probability = 0.25) and from low-latitude southern Pangaea to eastern and western north Pangaea (probability = 0.5). The Jurassic dispersal matrix was further modified to limit dispersal between eastern and western north Pangaea (probability = 0.25) to incorporate the breakup of northern Pangea. We used a stepping-stone model that allows for dispersal only between adjacent regions. We estimated maximum delta-log likelihood (hereafter, delta-likelihood)—the highest log likelihood across all dates for a single tree subtracted from the log likelihood for each date for a single tree—for each of the estimated time periods and used this to evaluate whether reduced dispersal from the arid belt resulted in higher or lower log likelihood for the entire model. A low delta-likelihood at a given time—relative to other sampled times—suggests that the model incorporating the arid belt is not well supported, that is, that there is little support for a biogeographic restriction at that time and that the phylogeny preserves evidence of dispersal across climatic zones. Conversely, a high delta-likelihood at a given time suggests that a restriction to dispersal is consistent with the phylogeny at that time, further suggesting that speciation events are primarily endemic and do not cross climatic barriers. Ancestral states under this model were estimated using the plot_BioGeoBEARS_results function with five different a posteriori dispersal matrices as suggested by likelihood reflecting (1) pre-arid belt, (2) arid belt, (3) arid belt dissipation, (4) arid belt return and (5) post-Triassic (using the same matrices as above), with start dates for the models selected from our previous analysis. To account for optimization errors, we used a generalized simulated annealing algorithm with the GenSA package (v.1.1.7)⁹², which samples the likelihood surface of complex models for a single global minimum, such that the model does not rest on local minima. Note that we interpret the greatly heightened delta-likelihood from -220–201 Ma (Fig. 3 and Extended Data Fig. 7) as partly artefactual: because the likelihood is driven by dispersal events, the greater number of endemic dispersal events within climatic zones later in the Triassic relative to the Carnian will cause the likelihood to be greater than that of the Carnian, even if the climatic barriers are comparable. Because of this, we are hesitant to interpret the greatly heightened delta-likelihood later in the Norian and Rhaetian at face value: although the signal unambiguously suggests heightened barriers to dispersal, as in the early Carnian, quantifying the intensity of these barriers relative to the early Carnian may be beyond the scope of the model to evaluate.

To test the sensitivity of our results to fossil sampling across Pangaea, we added hypothetical terminal taxa, assigned to be roughly the same

Article

age as *M. raathi* (that is, ‘Ischigualastian’ age), to test whether limited geographic sampling of early-diverging theropods, sauropodomorphs or herrerasaurids influenced the maximum-likelihood outcome of our biogeographic model. This simulates the potential for increased future sampling in other regions of Pangaea and allows us to test whether our model of dispersal is robust or driven primarily by limited sampling. All hypothetical taxa were added near the base of Sauropodomorpha, Theropoda and Herrerasauridae using the bind.tip command in the R package phytools (v.0.6-99)⁹³ in R (v.3.6.2)⁸⁶ and were temporally coincident with the earliest dinosaurs in our sample. We tested eight different permutations: all Ornithodira, Dinosauria only, one added theropod, three added theropods, one added sauropodomorph, three added sauropodomorphs, one added herrerasaurid, and one added herrerasaurid, theropod and sauropodomorph. All hypothetical taxa were placed in phylogenetic positions representing ‘worst-case scenarios’ for our hypothesis of early barriers to dinosaurian dispersal. Hypothetical taxa were placed both early in dinosaurian evolution and phylogenetically distant from each other to ensure multiple dispersal events during the Carnian and not one event for two closely related hypothetical taxa. Following this strategy, we placed hypothetical taxa as sister to early taxa or sister to extremely early nodes. The single hypothetical theropod was placed as sister to *Eodromaeus*, and the other two hypothetical theropods were placed sister to the unnamed node *Eodromaeus* + Neotheropoda and sister to all other theropods and were assigned an equatorial Pangaean provenance. The single hypothetical sauropodomorph was placed sister to *Saturnalia*, and the other two were likewise placed sister to the unnamed node *Buriolestes* + *Guaibasaurus* and to the unnamed node *Bagualosaurus* + Sauropoda and were assigned a northern Pangaean (both eastern and western) provenance. The hypothetical herrerasaurid was placed sister to *Herrerasaurus* and given a northern Pangaean (eastern and western) provenance. Crucially, the hypothetical taxa were assigned to geographic regions from which Carnian dinosaurs are not currently known; for example, the added sauropodomorph of Ischigualastian age was given a northern Pangaean provenance to explicitly test whether a lack of sampled Carnian sauropodomorphs from northern Pangaea would influence the results of our analyses. For each model, we calculated delta-likelihood as described above by subtracting the highest log likelihood returned for the entire sample from the log likelihood at each individual time period, such that results from each of the individual models were directly comparable. As an additional test of the limits of our hypothesis, we also tested a permutation with a hypothetical northern Carnian assemblage containing a greater diversity of early dinosaurs than any that has been recovered from southern Gondwana, with an added herrerasaurid, three added theropods and three added sauropodomorphs.

Early dinosaur phylogeny is controversial, with several competing hypotheses of relationships. To test the sensitivity of our biogeographic results to phylogenetic configuration, we ran the same analysis in BioGeoBEARS on 20 random trees taken from the posterior distribution of trees from the Bayesian analysis of the matrix in Langer et al., which include more likely configurations (for example, herrerasaurs as non-eusaurischians) and highly unlikely configurations (for example, Ornithischia and Sauropodomorpha united into a monophyletic Phytodinosauria, herrerasaurs outside Saurischia). Because of the computational demands of this analysis, we conducted this on the Virginia Tech Advanced Research Computing Cluster and accessed 128 nodes for 36 h, resulting in 4,608 total computational hours. We also conducted analyses on the Bayesian trees recovered from the matrices in Baron et al. and Cabreira et al. to further test how different phylogenetic arrangements might influence our results. Because the dating of the Pebbley Arkose Formation, although most likely late Carnian, is uncertain (Supplementary Information), we also conducted a biogeographic analysis with the Bayesian tree from Langer et al. (Fig. 3) with *Mbiresaurus* dated as early Norian (225 Ma) instead of late Carnian. Because our hypothesis of a theropod-first colonization

of northern Pangaea in the latest Carnian may be driven by a dearth of theropod taxa from South America during the earliest Norian, we conducted two analyses with a hypothetical South American theropod placed sister to the node *Tawa* + Neotheropoda and dated to the same age as *Bagualosaurus* in the first analysis and *Guaibasaurus* in the second analysis. Although the later sauropodomorphs *Lessemsaurus* and *Ingentia* were not included in any of the matrices we used to explore early dinosaurian relationships, their ages and hypothesized phylogenetic locations may make them influential to understanding the timing of Norian sauropodomorph evolution^{94,95}. These taxa were not available for us to score into the matrices we tested, so we again used the bind.tip command in the R package phytools (v.0.6-99)⁹³ to add *Lessemsaurus* and *Ingentia* to the phylogeny as each other’s closest relative, sister to *Antetonitrus*⁹⁴, with Norian sauropodomorph divergence times adjusted accordingly. The results of all these analyses can be found in Extended Data Fig. 7.

Because dinosaurian dispersal from southern Pangaea was our primary focus, our model was centred on testing for limited dispersal through low-latitude southern Pangaea, where an arid belt has been proposed to have acted as a barrier to dispersal through most of the Late Triassic¹⁸. However, a similar arid belt was also present in the low latitudes of northern Pangaea¹⁷, north of equatorial Pangaea, and this belt has similarly been proposed to have acted as a barrier to dispersal during the Late Triassic¹⁸ (Fig. 1a). To test how inclusion of this northern belt affected our model, we ran the same biogeographic dispersal analysis but with the dispersal rate between equatorial Pangaea and northern Pangaea (eastern and western north Pangaea) changed from 1 to 0.5 (Extended Data Fig. 7).

Sources for silhouettes and reconstructions

The *Mbiresaurus raathi* skeletal reconstruction was by S. Hartman (used with permission); the *M. raathi* silhouette was based on this reconstruction. The hyperodapedontine rhynchosaur silhouette was by M. Garcia (used with permission). The cynodont silhouette was created by C.T.G. Other silhouettes are licensed under a Creative Commons Attribution 3.0 Unported license (<https://creativecommons.org/licenses/by/3.0/>) and are by S. Hartman (herrerasaurid and aetosaur) or were modified from artwork by D. Bogdanov (dicynodont).

Reporting summary

Further information on research design is available in the Nature Research Reporting Summary linked to this article.

Data availability

All data files used for analyses are hosted on Dryad (<https://doi.org/10.5061/dryad.pg4f4qrqd>). All fossils are reposed in recognized natural history institutions. To preserve the integrity of the fossil localities and the natural history resources of Zimbabwe, we do not present the geographic coordinate data here. Geographic coordinate data are available on request from the NHMZ and are recorded in the specimen catalogue and records of the NHMZ for full reproducibility. This publication and associated nomenclatural acts have been registered in ZooBank as urn:lsid:zoobank.org:pub:BE5720A6-9CE6-48A0-A232-32A01CC551B0.

Code availability

All code used in this study has been deposited in Dryad (<https://doi.org/10.5061/dryad.pg4f4qrqd>).

61. Baron, M. G., Norman, D. B. & Barrett, P. M. Baron et al. reply. *Nature* **551**, E4–E5 (2017).
62. Nesbitt, S. J. & Sues, H.-D. The osteology of the early-diverging dinosaur *Daemonosaurus chauliodus* (Archosauria: Dinosauria) from the Coelophysis Quarry (Triassic: Rhaetian) of New Mexico and its relationships to other early dinosaurs. *Zool. J. Linnean Soc.* **191**, 0150–179 (2020).

63. Baron, M. G. *Pisanosaurus mertii* and the Triassic ornithischian crisis: could phylogeny offer a solution? *Hist. Biol.* **31**, 967–981 (2019).
64. Benton, M. J. & Walker, A. D. *Saltopus*, a dinosauriform from the Upper Triassic of Scotland. *Earth Environ. Sci. Trans. R. Soc. Edin.* **101**, 285–299 (2010).
65. Nesbitt, S. J., Barrett, P. M., Werning, S., Sidor, C. A. & Charig, A. J. The oldest dinosaur? A Middle Triassic dinosauriform from Tanzania. *Biol. Lett.* **9**, 20120949 (2013).
66. Agnolin, F. L. & Ezcurra, M. D. The validity of *Lagosuchus talampayensis* Romer, 1971 (Archosauria, Dinosauriformes), from the Late Triassic of Argentina. *Breviora* **565**, 1–21 (2019).
67. Goloboff, P. A., Farris, J. S. & Nixon, K. C. TNT, a free program for phylogenetic analysis. *Cladistics* **24**, 774–786 (2008).
68. Mesquite: a modular system for evolutionary analysis v.3.70 (2021).
69. Goloboff, P. A. & Szumik, C. A. Identifying unstable taxa: efficient implementation of triplet-based measures of stability, and comparison with Phyutility and RogueNaRok. *Mol. Phylogenet. Evol.* **88**, 93–104 (2015).
70. Wagner, P. J. A likelihood approach for evaluating estimates of phylogenetic relationships among fossil taxa. *Paleobiology* **24**, 430–449 (1998).
71. Kolaczkowski, B. & Thornton, J. W. Performance of maximum parsimony and likelihood phylogenetics when evolution is heterogeneous. *Nature* **431**, 980–984 (2004).
72. Goloboff, P. A., Pittman, M., Pol, D. & Xu, X. Morphological data sets fit a common mechanism much more poorly than DNA sequences and call into question the Mkv model. *Syst. Biol.* **68**, 494–504 (2019).
73. Goloboff, P. A., Torres, A. & Arias, J. S. Weighted parsimony outperforms other methods of phylogenetic inference under models appropriate for morphology. *Cladistics* **34**, 407–437 (2018).
74. Goloboff, P. A., Torres Galvis, A. & Arias, J. S. Parsimony and model-based phylogenetic methods for morphological data: comments on O'Reilly et al. *Palaeontology* **61**, 625–630 (2018).
75. Kammerer, C. F., Nesbitt, S. J., Flynn, J. J., Ranivoharimana, L. & Wyss, A. R. A tiny ornithodiran archosaur from the Triassic of Madagascar and the role of miniaturization in dinosaur and pterosaur ancestry. *Proc. Natl Acad. Sci. USA* **117**, 17932–17936 (2020).
76. Ezcurra, M. D. et al. Enigmatic dinosaur precursors bridge the gap to the origin of Pterosauria. *Nature* **588**, 445–449 (2020).
77. Parry, L. A., Baron, M. G. & Vinther, J. Multiple optimality criteria support Ornithoscelida. *R. Soc. Open Sci.* **4**, 170833 (2017).
78. O'Reilly, J. E. et al. Bayesian methods outperform parsimony but at the expense of precision in the estimation of phylogeny from discrete morphological data. *Biol. Lett.* **12**, 20160081 (2016).
79. Koch, N. M., Garwood, R. J. & Parry, L. A. Fossils improve phylogenetic analyses of morphological characters. *Proc. Royal Soc. B Biol. Sci.* **288**, 20210044 (2021).
80. Bouckaert, R. et al. BEAST 2.5: an advanced software platform for Bayesian evolutionary analysis. *PLoS Comput. Biol.* **15**, e1010650 (2019).
81. Drummond, A. J. & Suchard, M. A. Bayesian random local clocks, or one rate to rule them all. *BMC Biol.* **8**, 114 (2010).
82. Rambaut, A., Drummond, A. J., Xie, D., Baele, G. & Suchard, M. A. Posterior summarization in Bayesian phylogenetics using Tracer 1.7. *Syst. Biol.* **67**, 901–904 (2018).
83. Drummond, A. J. & Rambaut, A. BEAST: Bayesian evolutionary analysis by sampling trees. *BMC Evol. Biol.* **7**, 214 (2007).
84. Landis, M., Edwards, E. J. & Donoghue, M. J. Modeling phylogenetic biome shifts on a planet with a past. *Syst. Biol.* **70**, 86–107 (2020).
85. Landis, M. J., Freymen, W. A. & Baldwin, B. G. Retracing the Hawaiian silversword radiation despite phylogenetic, biogeographic, and paleogeographic uncertainty. *Evolution* **72**, 2343–2359 (2018).
86. R Core Team. *R: A Language and Environment for Statistical Computing* (R Foundation for Statistical Computing, 2020).
87. Matzke, N. J. Probabilistic historical biogeography: new models for founder-event speciation, imperfect detection, and fossils allow improved accuracy and model-testing. *Front. Biogeogr.* **5**, 242–248 (2013).
88. Matzke, N. J. Model selection in historical biogeography reveals that founder-event speciation is a crucial process in island clades. *Syst. Biol.* **63**, 951–970 (2014).
89. Ree, R. H. & Sanmartín, I. Conceptual and statistical problems with the DEC+J model of founder-event speciation and its comparison with DEC via model selection. *J. Biogeogr.* **45**, 741–749 (2018).
90. Aberhan, M. Bivalve palaeobiogeography and the Hispanic Corridor: time of opening and effectiveness of a proto-Atlantic seaway. *Palaeogeogr. Palaeoclimatol. Palaeoecol.* **165**, 375–394 (2001).
91. Schöllhorn, I. et al. Climate and environmental response to the break-up of Pangea during the Early Jurassic (Hettangian-Piennsachian); the Dorset coast (UK) revisited. *Glob. Planet. Change* **185**, 103096 (2020).
92. Xiang, Y., Gubian, S., Suomela, B. & Hoeng, J. Generalized simulated annealing for global optimization: the GenSA package. *R J.* **5**, 13–28 (2013).
93. Revell, L. J. phytools: an R package for phylogenetic comparative biology (and other things). *Methods Ecol. Evol.* **3**, 217–223 (2012).
94. Apaldetti, C., Martínez, R. N., Cerda, I. A., Pol, D. & Alcober, O. An early trend towards gigantism in Triassic sauropodomorph dinosaurs. *Nat. Ecol. Evol.* **2**, 1227–1232 (2018).
95. Pol, D., Otero, A., Apaldetti, C. & Martínez, R. N. Triassic sauropodomorph dinosaurs from South America: the origin and diversification of dinosaur dominated herbivorous faunas. *J. South Amer. Earth Sci.* **107**, 103145 (2021).
96. Melo, T. P., Abdala, F. & Soares, M. B. The Malagasy cynodont *Menadon besairiei* (Cynodontia; Traversodontidae) in the Middle–Upper Triassic of Brazil. *J. Vertebr. Paleontol.* **35**, e1002562 (2015).
97. Parker, W. G. Revised phylogenetic analysis of the Aetosauria (Archosauria: Pseudosuchia); assessing the effects of incongruent morphological character sets. *PeerJ* **4**, e1583 (2016).
98. Parker, W. G. Redescription of *Calyptosuchus (Stagonolepis) wellesi* (Archosauria: Pseudosuchia: Aetosauria) from the Late Triassic of the Southwestern United States with a discussion of genera in vertebrate paleontology. *PeerJ* **6**, e4291 (2018).
99. Roberto-da-Silva, L. et al. A new aetosaur from the Upper Triassic of the Santa Maria Formation, southern Brazil. *Zootaxa* **3764**, 240–278 (2014).
100. Alcober, O. A. & Martínez, R. N. A new herrerasaurid (Dinosauria, Saurischia) from the Upper Triassic Ischigualasto Formation of northwestern Argentina. *Zookeys* **19**, 55–81 (2010).
101. Brinkman, D. B. & Sues, H.-D. A staurikosaurid dinosaur from the Upper Triassic Ischigualasto Formation of Argentina and the relationships of the Staurikosauridae. *Palaeontology* **30**, 493–503 (1987).
102. Pacheco, C. et al. *Gnathovorax cabreirai*: a new early dinosaur and the origin and initial radiation of predatory dinosaurs. *PeerJ* **7**, e7963 (2019).
103. Angielczyk, K. D., Hancox, P. J. & Nabavizadeh, A. A redescription of the Triassic kannemeyeriiform dicynodont *Sangsaurus* (Therapsida, Anomodontia), with an analysis of its feeding system. *J. Vertebr. Paleontol.* **37**, 189–227 (2017).
104. Langer, M. C., da Rosa, Á. A. S. & Montefeltro, F. C. *Supradapedon* revisited: geological explorations in the Triassic of southern Tanzania. *PeerJ* **5**, e4038 (2017).
105. Montefeltro, F. C., Langer, M. C. & Schultz, C. L. Cranial anatomy of a new genus of hyperodapedontine rhynchosaur (Diapsida, Archosauromorphia) from the Upper Triassic of southern Brazil. *Earth Environ. Sci. Trans. R. Soc. Edin.* **101**, 27–52 (2010).

Acknowledgements We thank M. Fitzpatrick and the NHMZ for access to collections and for fieldwork logistics, National Museums and Monuments of Zimbabwe for field logistic assistance, the Research Council of Zimbabwe for foreign researcher permits and the Zimbabwe Geological Survey for mapping information. We acknowledge the Broderick family for help with field logistics. We thank local and regional Zimbabwean authorities (Communal Areas Management Programme for Indigenous Resources (CAMPFIRE), Mushumbi Pools Police, Mbire Rural Council, Mbire District Tsetse Control, Mbire District Development Coordinator) for accommodating fieldwork. We acknowledge the people of Dande, on whose Communal Land this research was conducted. We thank K. Rose, T. Oishi, B. Chermak, D. Chermak, G. Iannaccone and V. Yarborough for fossil preparation. We thank E. Mbambo, K. Madzana and G. Malunga for fieldwork assistance and Z. Murphy and L. Broderick for documentary assistance. We thank M. Stocker, S. Xiao, J. Uyeda, M. Raath, M. Landis, A. Bhullar, J. Gauthier, the Virginia Tech Paleobiology Research Group, J. Choiniere, W. Parker, K. Angielczyk, T. Melo, V. Paes-Neto, L. Corecco, C. Schultz, M. Bronzati, J. Marsola, M. Garcia, B. McPhee, F. Montefeltro and the other students/postdocs of USP Ribeirão Preto and UFRGS for discussion. We thank the following collections managers and institutions: M. Bamford, B. Zipfel, BPI (now ESI); Z. Skosan Erasmus, N. Mtalana, SAM; C. Schultz, UFRGS; A. M. Ribeiro, MCN; M. B. de Andrade, MCP. The Willi Hennig Society provided TNT software free of charge. We acknowledge Advanced Research Computing at Virginia Tech (<https://arc.vt.edu/>) for providing computational resources and technical support that contributed to our results. This work was supported by a National Geographic Society Early Career Grant (CP-R004-17), a National Science Foundation Graduate Research Fellowship, a Geological Society of America Graduate Student Research Grant, a Paleontological Society Arthur J. Boucot Student Research Award, two Virginia Tech Graduate School Graduate Research Development Program awards, a Virginia Tech Department of Geosciences Summer Scholarship (all to C.T.G.), a National Geographic Society Exploration Grant (NGS-157R-18, to C.T.G. and S.J.N.) and Fundação de Amparo à Pesquisa do Estado de São Paulo (FAPESP 2020/07997-4, to M.C.L.).

Author contributions C.T.G. and S.J.N. designed the research project; C.T.G., D.M., T.J.B., S.T. and S.J.N. designed the field project; D.M. conducted fieldwork and permit logistics with C.T.G., C.T.G., D.M., T.J.B., M.Z., S.T., S.J.N. and H.R.T. conducted fieldwork; B.M.W. conducted the phylogenetic analyses and the ancestral state estimation and constructed the biogeographic dispersal model with input from C.T.G., M.C.L. and S.J.N.; D.M. and T.J.B. conducted geological and stratigraphic mapping; C.T.G. conducted histological analysis; C.T.G., M.C.L. and S.J.N. assembled the differential diagnosis; D.M. composed the Shona-language summary and M.Z. composed the Ndebele-language summary; C.T.G. wrote the manuscript with contributions from all authors.

Competing interests The authors declare no competing interests.

Additional information

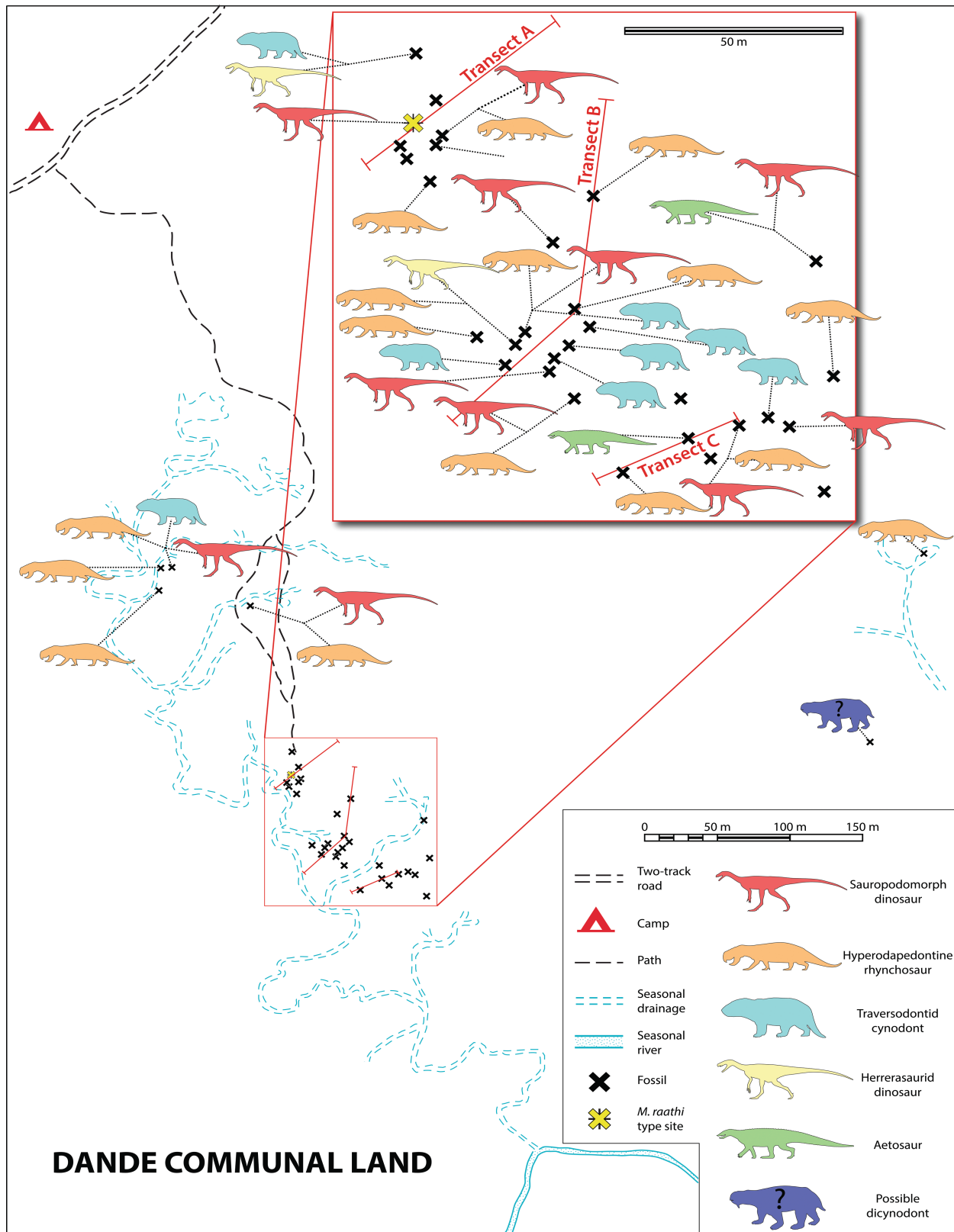
Supplementary information The online version contains supplementary material available at <https://doi.org/10.1038/s41586-022-05133-x>.

Correspondence and requests for materials should be addressed to Christopher T. Griffin.

Peer review information *Nature* thanks Martin Ezcurra, Diego Pol and the other, anonymous, reviewer(s) for their contribution to the peer review of this work.

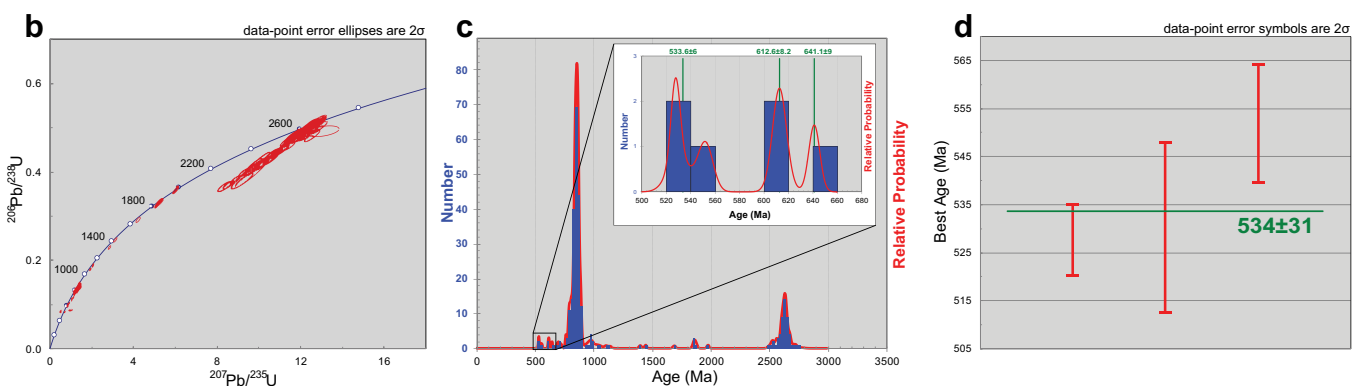
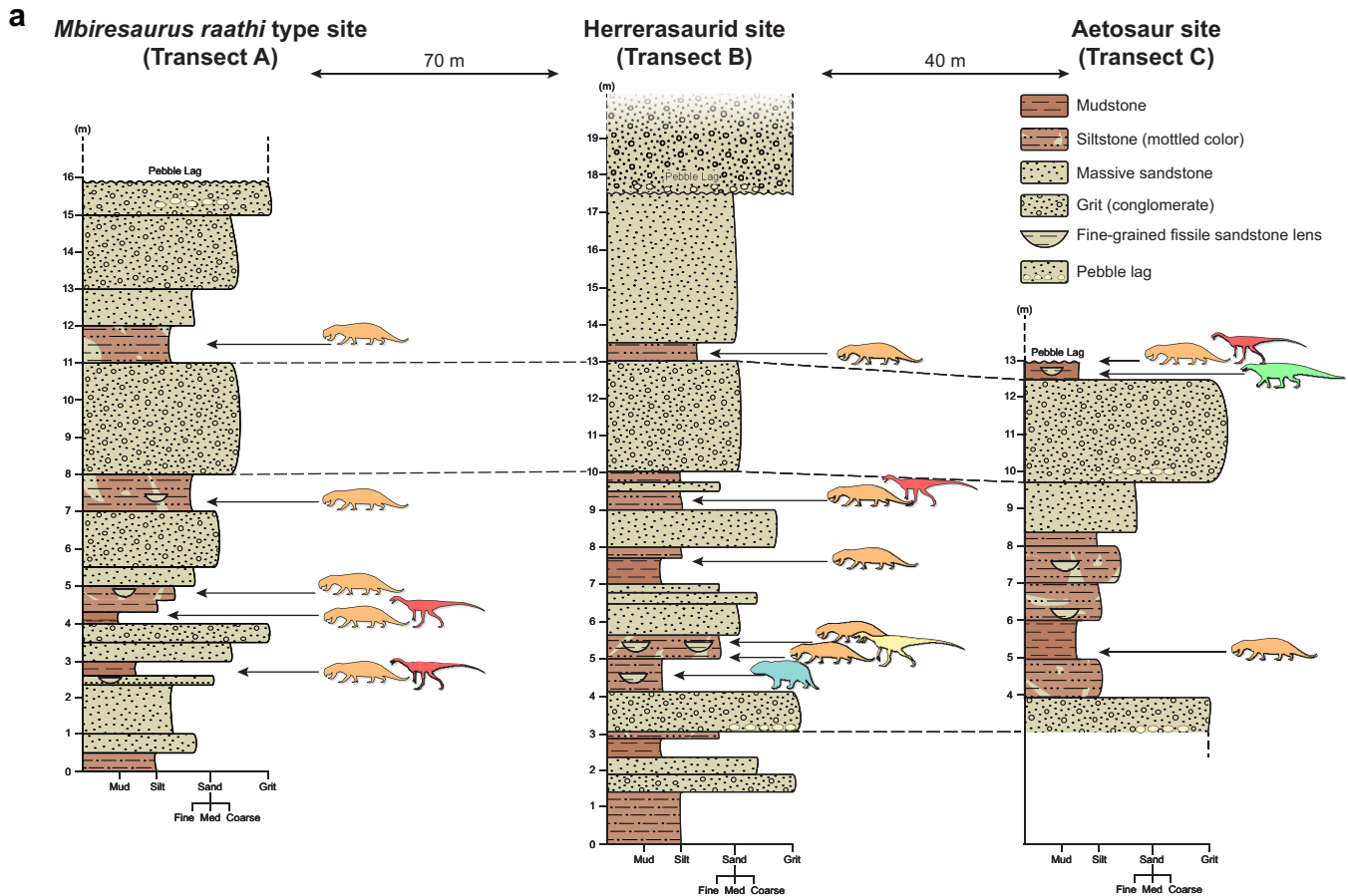
Reprints and permissions information is available at <http://www.nature.com/reprints>.

Article



Extended Data Fig. 1 | Map of individual fossil localities from the most productive region of the Pebby Arkose Fm., Dande Communal Area, Zimbabwe. Localities without an accompanying silhouette represent

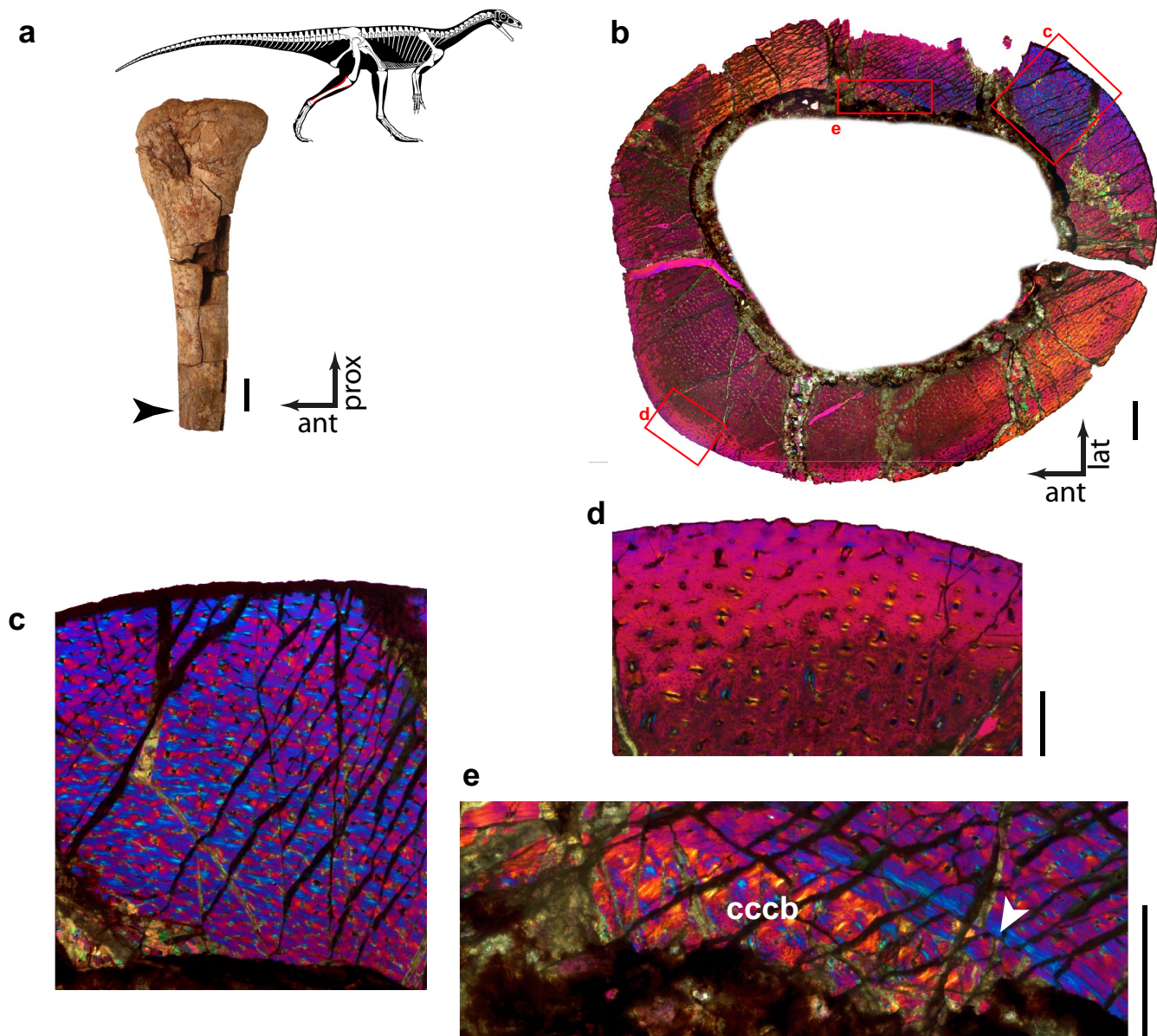
unidentified bone fragments. Version of map with latitude and longitude available on request through C.T.G. and the NHMZ.



Extended Data Fig. 2 | Stratigraphic columns and detrital zircon dating information from the Pebby Arkose Fm., Dande Communal Area, Zimbabwe. **a**, Stratigraphic columns of three transects (Extended Data Fig. 1) showing that taxa from the Dande assemblage are present in multiple stratigraphic layers in this region. **b**, Concordia plot of ^{238}U - ^{206}Pb ratios against ^{235}U - ^{207}Pb ratios of detrital zircons from the Pebby Arkose Fm., Dande

Communal Area, Zimbabwe. Error ellipses are error at 2 σ . **c**, Detrital zircon age distribution, indicating the youngest grains in the sample are ~534 Ma. **d**, Best maximum age for the detrital zircon distribution is ~534 Ma, indicating the processes that created these zircons occurred long before the deposition of our Carnian locality. Error bars are standard error at 2 σ ; n = 275 independent measurements.

Article



Extended Data Fig. 3 | Bone histology of *Mbiresaurus raathi*, gen. et sp. nov.
a, Right tibia of *Mbiresaurus raathi* holotype (NHMZ 2222) in medial view (red element in skeletal reconstruction). Arrow indicates location of histological sampling. **b**, Whole-slide image of tibial histology of NHMZ 2222 under cross-polarized light with waveplate. **c**, Posterolateral portion of the tibial cortex under cross-polarized light with waveplate. **d**, Sub-periosteal tissue of the anteromedial portion of the cortex under cross-polarized light with

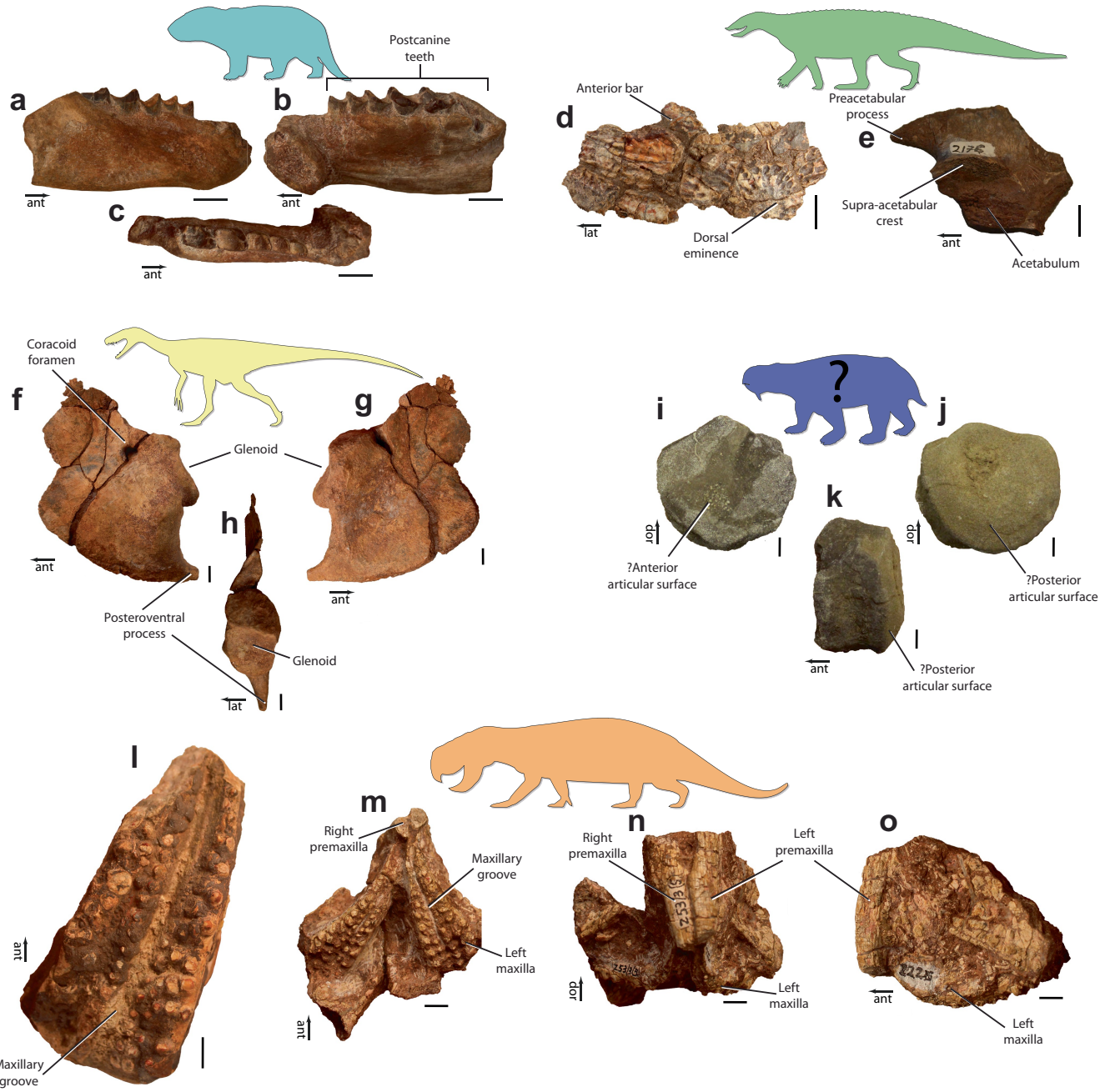
waveplate. **e**, Internal portion of the cortex showing original endosteal lamellae and compact coarse cancellous bone formed via cortical drift under cross-polarized light with waveplate. Arrow indicates endosteal lamellae (i.e., inner circumferential layer). ant, anterior; cccb, compact coarse cancellous bone; prox, proximal; lat, lateral. Scale bars, **a**, 1 cm, **b**, 1 mm, **c**, 500 µm, **d**, 250 µm, **e**, 500 µm.



Extended Data Fig. 4 | Maximum clade credibility trees returned by Bayesian phylogenetic inference, and strict and reduced strict consensus trees returned by parsimony-based phylogenetic analyses. **a**, Maximum clade credibility (MCC) tree of the Bayesian analysis of the Baron et al.^{39,61–63} matrix. Posterior probabilities for each node reported in the online supplement. **b**, MCC tree of the Bayesian analysis of the Cabreira et al.²⁶ matrix. Posterior probabilities for each node reported in the online supplement. **c**, MCC tree of the Bayesian Langer et al.⁵³ matrix, including *Saltopus*. Posterior probabilities for each node reported in the online supplement. **d**, Reduced strict consensus of the Langer et al.⁵³ parsimony analysis, excluding character 217 (61,408 MPTs of 1,958 steps; CI = 0.269, RI = 0.617). Strict consensus and supporting synapomorphies reported in the online supplement. **e**, Reduced strict consensus of the Langer et al.⁵³ parsimony analysis, excluding character 217 and the taxa *Saltopus*, *Agnosophitys*, and *Nyasasaurus* (99,999 [memory overflow] MPTs of 1,942 steps; CI = 0.271, RI = 0.621). Strict consensus and

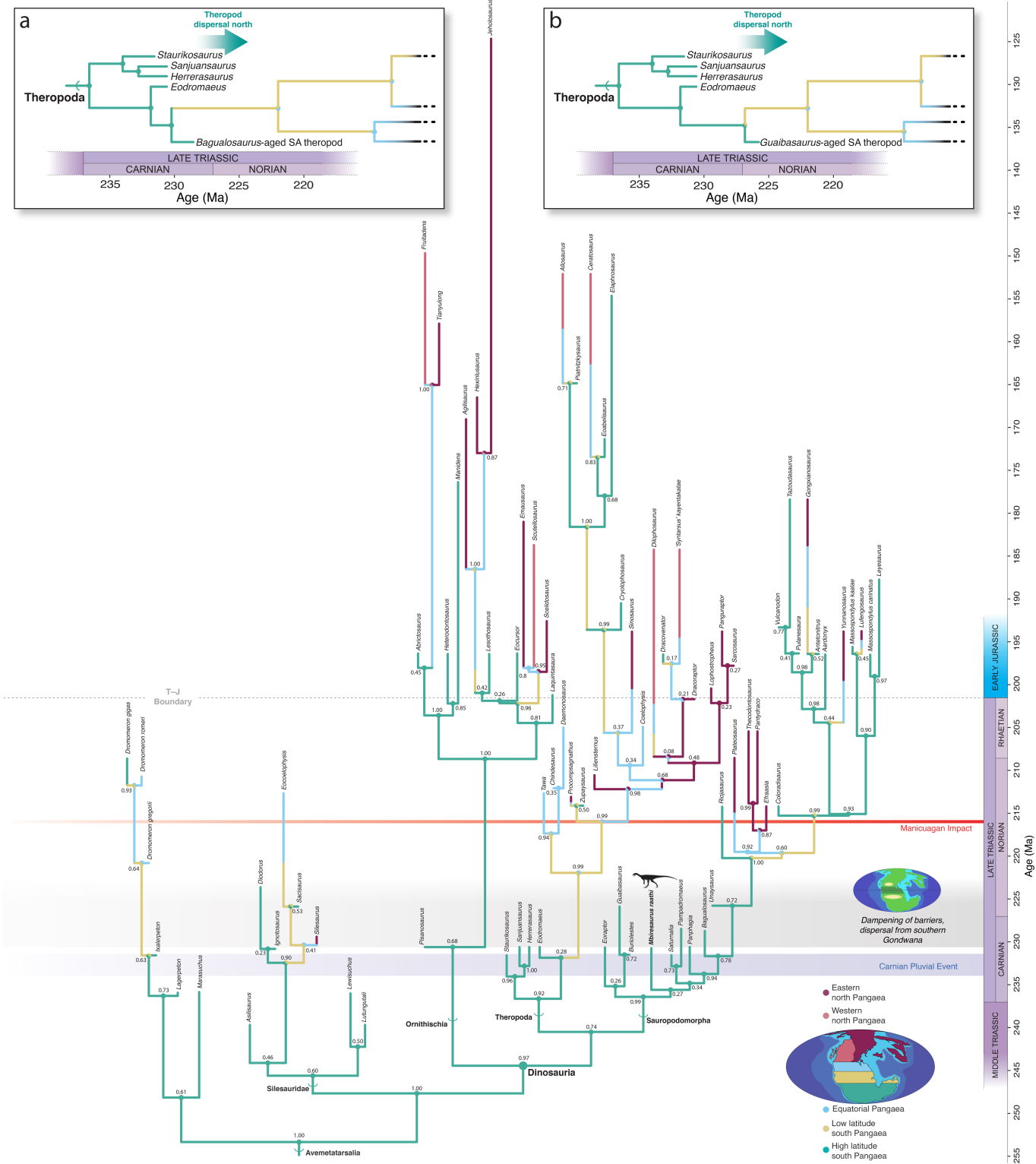
supporting synapomorphies reported in the online supplement. **f**, Reduced strict consensus of the Baron et al.^{39,61–63} parsimony analysis, excluding character 217 (99,999 [memory overflow] MPTs of 1,923 steps; CI = 0.274, RI = 0.615). Strict consensus and supporting synapomorphies reported in the online supplement. **g**, Reduced strict consensus of the Baron et al.^{39,61–63} parsimony analysis, excluding character 217 and the taxa *Saltopus*, *Agnosophitys*, and *Nyasasaurus* (61,680 MPTs of 1,907 steps; CI = 0.276, RI = 0.619). Strict consensus and supporting synapomorphies reported in the online supplement. **h**, Reduced strict consensus of the Cabreira et al.²⁶ parsimony analysis (336 MPTs of 866 steps; CI = 0.336, RI = 0.631). Strict consensus and supporting synapomorphies reported in the online supplement. **i**, Reduced strict consensus of the Cabreira et al.²⁶ parsimony analysis excluding *Saltopus* (84 MPTs of 861 steps; CI = 0.338, RI = 0.634). Strict consensus and supporting synapomorphies reported in the online supplement.

Article



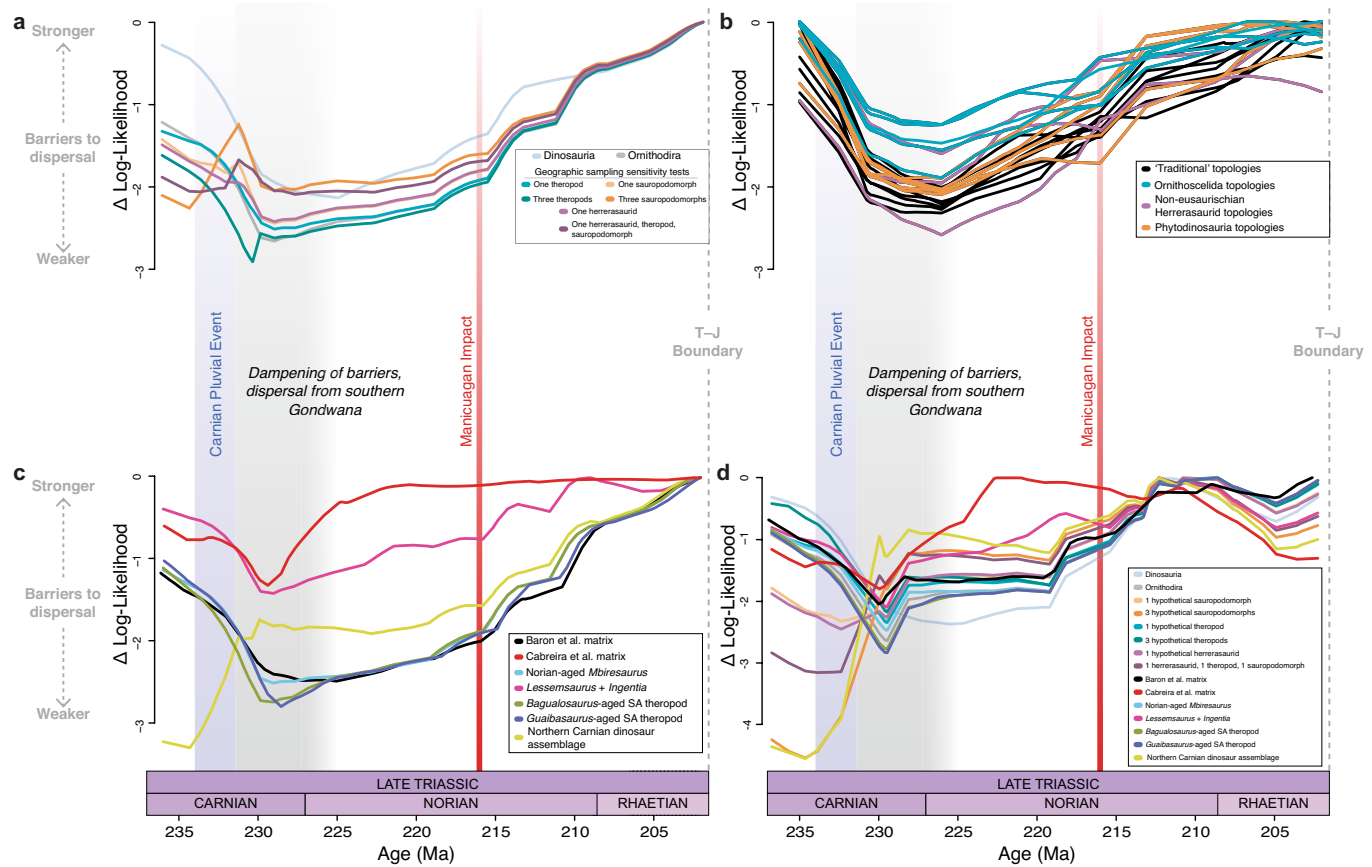
Extended Data Fig. 5 | Diagnostic features of the Pebby Arkose Fm. assemblage, Dande Communal Area. **a–c,** Gomphodontosuchine traversodontid cynodont, right dentary, **a**, lateral, **b**, medial, **c**, occlusal view. Gomphodontosuchine synapomorphies⁹⁶ include: anterolingual cusp of lower postcanines strongly posteriorly inclined, procumbent lower incisors, reduced lower canine, labial cusp widest in transverse row of lower postcanines. **d–e,** Aetosaur, **d**, left paramedian osteoderm in dorsal view, **e**, left ilium in lateral view. Aetosaurian synapomorphies⁹⁷ include: anterior bar on paramedian osteoderm, radiate pattern of ornamentation on paramedian osteoderm. The triangular preacetabular process of the ilium is similar to many early aetosaurs^{97–99}. **f–h,** Herrerasaurid dinosaur, coracoid, **f**, lateral, **g**, medial, **h**, posterodorsal view. As in other herrerasaurids^{48,100–102}, there is a long hook-like posteroventral process and the coracoid foramen is anteroventral to the glenoid. **i–k,** Possible dicynodont, highly weathered trunk vertebra centrum, **i**, ?anterior, **j**, ?posterior, **k**, ?left lateral view. The size and general shape of the centrum (amphicoelous, anteroposteriorly compressed,

articular surfaces taller and wider than body) is consistent with those of kannemeyeriform dicynodonts¹⁰³. **l,** Hyperodapedontine rhynchosaur, large left maxilla in occlusal view. **m–o,** Hyperodapedontine rhynchosaur, smaller articulated maxillae and premaxillae originally reported by Raath et al.²⁹, **m**, occlusal, **n**, anterior, **o**, left lateral view. The maxillary groove is a rhynchosaurid synapomorphy¹⁰⁴. Hyperodapedontine synapomorphies¹⁰⁴ include: broader than deep tooth-bearing area of maxilla; ‘Hyperodapedon clade’ synapomorphies¹⁰⁴ include: > 2 tooth rows medial to maxillary groove. This rhynchosaur lacks synapomorphies of the *Teyumbaita* clade of hyperodapedontine rhynchosaurids (*T. sulcognathus*¹⁰⁵ and *T. sp*⁵⁴): two maxillary grooves that extend anteriorly beyond the posterior third of the tooth plate (the Zimbabwean form has only one maxillary groove); maxillary area lateral to main groove narrower than the medial area (also present in *H. hunei*; proportions reversed in Zimbabwean form). Scale bars 1 cm. ant, anterior; dor, dorsal; lat, lateral.



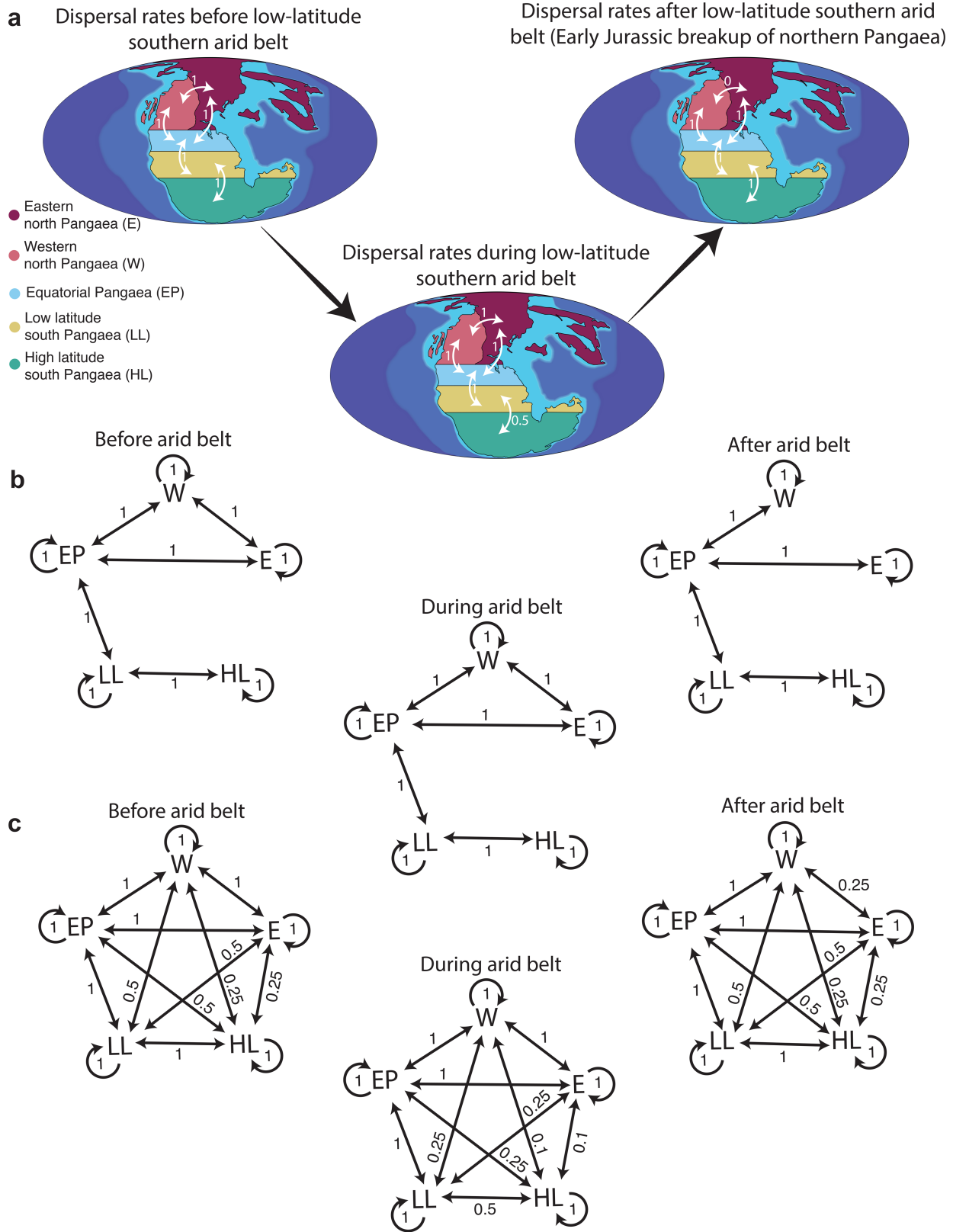
Extended Data Fig. 6 | Full ornithodiran phylogeny and ancestral state estimations. The entire ornithodiran phylogeny recovered by Bayesian analysis of the Langer et al.⁵³ dataset. We follow Ezcurra et al.⁷⁶ and Kammerer et al.⁷⁵ in considering Lagerpetids as early pterosauromorphs, such that the Lagerpetidae + Dinosauria node is considered Ornithodira. Numbers at nodes indicate posterior probabilities to two significant digits. **a.** Ancestral state estimation if a *Bagualosaurus*-aged early theropod is recovered from southern Pangaea (e.g.,

Article



Extended Data Fig. 7 | Biogeographic dispersal model with individual results of sampling sensitivity tests. **a**, The dispersal pattern of early dinosaurs from high-latitude southern Pangaea is robust to the possibility of increased sampling of Carnian dinosaurs in other regions of Pangaea; the same general pattern of restriction, dispersal, and later restriction holds with the addition of hypothetical sampling elsewhere in Pangaea. **b**, The dispersal pattern of early dinosaurs from high-latitude southern Pangaea is consistent among differing phylogenetic topologies—20 trees taken from the posterior distribution of trees from the Langer et al. Bayesian analysis show consistent patterns even given a wide variety of topologies. **c**, The dispersal pattern of early dinosaurs from high-latitude southern Pangaea is consistent among differing

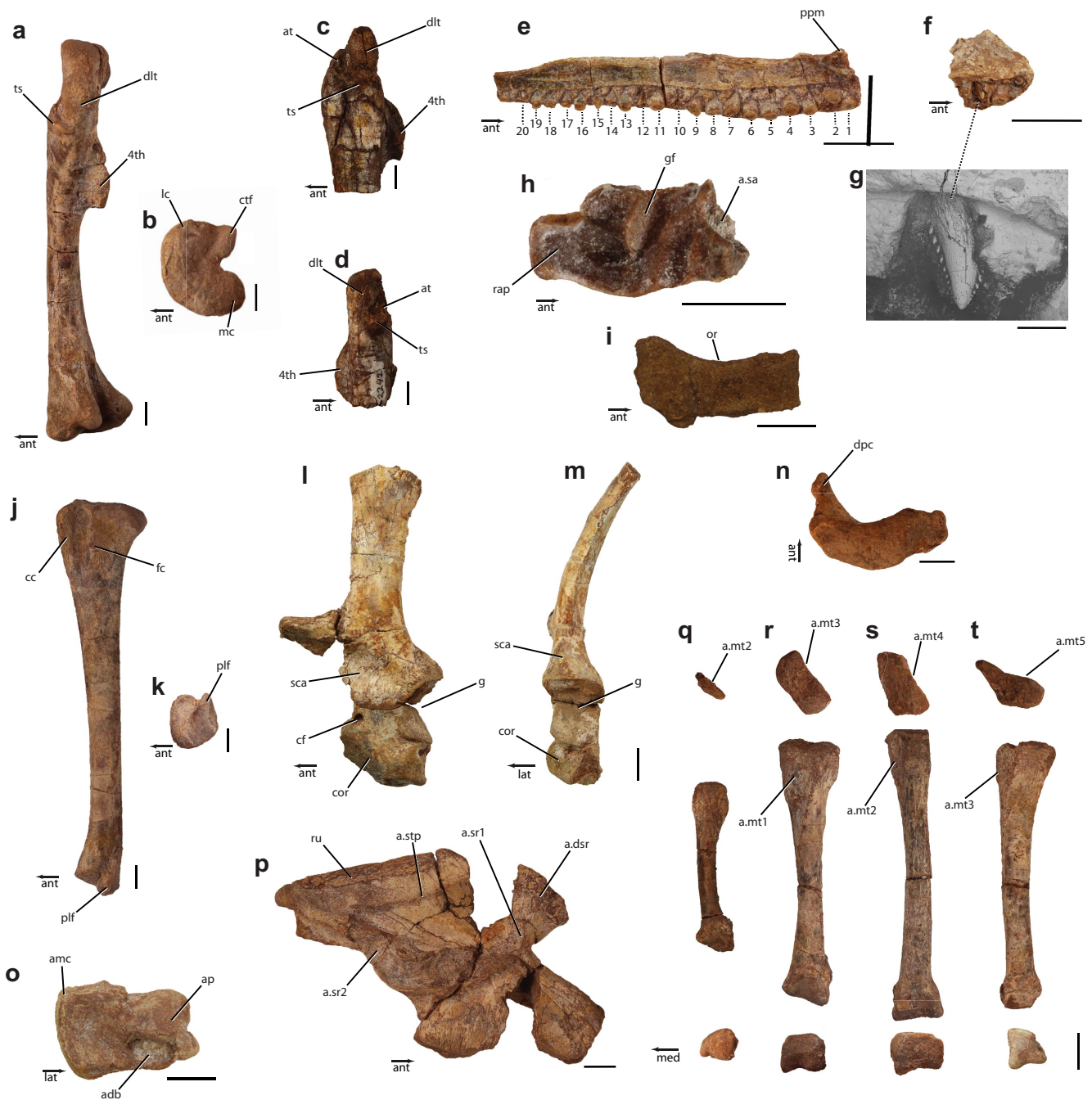
phylogenetic topologies and sensitivity analyses, including the Baron et al. and Cabreira et al. Bayesian trees, if *Mbiresaurus raathi* is Norian in age, if *Lessemsaurus* and *Ingentia* are included in the analysis, and if *Bagualosaurus* or *Guaibasaurus*-aged theropods are recovered from South America. Our hypothesis will be falsified if an extremely diverse dinosaurian assemblage is recovered from the Carnian of northern Pangaea (northern Carnian dinosaur assemblage). **d**, Results of the model variant simulating arid belts in the tropics of both northern and southern Pangaea (see Methods); the same general pattern holds, and this pattern is disrupted a diverse hypothetical northern dinosaurian assemblage, and three hypothetical northern sauropodomorphs.



Extended Data Fig. 8 | Dispersal rates for the biogeographic dispersal model. **a**, Overall dispersal rates, shown between the different regions of Pangaea. **b**, The dispersal rates used to define the stepping stone model. **c**, The dispersal rates used to test for differential dispersal in response to low-latitude

climatic barrier and the breakup of northern Pangaea. Note that in our model variant simulating a northern Pangaeian arid belt (see Methods), the $E \leftrightarrow EP$ and $W \leftrightarrow EP$ rates were changed from 1 to 0.5.

Article



Extended Data Fig. 9 | Further skeletal anatomy of *Mbiresaurus raathi*, gen. et sp. nov. Except where noted, all specimens are the holotype (NHMZ 2222). **a**, Left femur, lateral view. **b**, Left femur, distal view. **c**, Left femur, potentially referable to *Mraathi* (NHMZ 2223), lateral view. **d**, Right femur, potentially referable to *Mraathi* (NHMZ 2242), lateral view. **e**, Left maxilla, occlusomedial view, teeth are numbered. **f**, Left premaxilla, occlusomedial view. **g**, Scanning electron microscope image of premaxillary tooth 4. **h**, Right articular, dorsal view. **i**, Unprepared right frontal, dorsal view, showing frontal proportions (NHMZ 2222). **j**, Right tibia, lateral view. **k**, Right tibia, distal view. **l**, Left scapula and coracoid (NHMZ 2547), lateral view. **m**, Left scapula and coracoid (NHMZ 2547), posterior view. **n**, Left humerus, proximal view. **o**, Right astragalus, proximal view. **p**, Left ilium (NHMZ 2547), medial view. **q**, Left metatarsal I, proximal (top), anterior (middle), distal (bottom) views. **r**, Left metatarsal II, proximal (top), anterior (middle), distal (bottom) views. **s**, Left

metatarsal III, proximal (top), anterior (middle), distal (bottom) views. **t**, Left metatarsal IV, proximal (top), anterior (middle), distal (bottom) views. Scale bars, **a-f**, **h-t**, 1 cm; **g**, 1 mm. 4th, fourth trochanter; **a**, articulates with; **adb**, dorsal basin of astragalus; **amc**, anteromedial corner; **ap**, ascending process; **at**, anterior trochanter; **ant**, anterior; **cc**, cnemial crest; **cf**, coracoid foramen; **cor**, coracoid; **ctf**, crista tibiofibularis; **dlt**, dorsolateral trochanter; **dpc**, deltopectoral crest; **dsr**, sacral rib of dorsosacral; **fc**, fibular crest; **g**, glenoid of scapula and coracoid; **gf**, glenoid fossa of the articular; **lat**, lateral; **lc**, lateral condyle; **mc**, medial condyle; **mt#**, metatarsal #; **or**, orbital rim; **plf**, posterolateral flange; **ppm**, palatal process of the maxilla; **rap**, retroarticular process; **ru**, rugosity; **sa**, surangular; **sca**, scapula; **sr1**, sacral rib of primordial sacral 1; **sr2**, sacral rib of primordial sacral 2; **stp**, transverse processes of sacral vertebrae; **ts**, trochanteric shelf.



Extended Data Fig. 10 | See next page for caption.

Article

Extended Data Fig. 10 | Further comparative skeletal anatomy of *Mbiresaurus raathi*, gen. et sp. nov. **a**, Left ilium, *Mbiresaurus raathi* (NHMZ 2547), lateral view. **b**, Right ilium (reversed), *Buriolestes schultzi* (ULBRA-PVT280), lateral view. **c**, Right ilium (reversed), *Saturnalia tupiniquim* (MCP 3846-PV), lateral view. **d**, Left ilium, *Panphagia protos* (PVSJ 874), lateral view. **e**, Left ilium, *Adeopapposaurus mognai* (PVSJ 569), lateral view. **f**, Left ilium, *Plateosaurus engelhardti* (SMNS 91310), lateral view. **g**, Right dentary, *Mbiresaurus raathi* (NHMZ 2222), medial view. **h**, Left dentary (reversed), *Mbiresaurus raathi* (NHMZ 2222), medial view. **i**, Left dentary (reversed), *Mbiresaurus raathi* (NHMZ 2222), lateral view. **j**, Right dentary, *Mbiresaurus raathi* (NHMZ 2222), lateral view. **k**, Right premaxilla, maxilla, and dentary, *Eoraptor lunensis* (PVSJ 512), lateral view. **l**, Right dentary, *Saturnalia tupiniquim* (UFSM 17614), lateral view. **m**, Left ulna, *Mbiresaurus raathi* (NHMZ 2222), lateral view. **n**, Right ulna (reversed), *Saturnalia tupiniquim* (MCP 3844-PV); Institutional abbreviations in online supplement. **o**, Right scapula, *Mbiresaurus raathi* (NHMZ 2547), lateral view. **p**, Left scapula (reversed), *Panphagia protos* (PVSJ 874), lateral view. **q**, Left femur, proximal end, *Mbiresaurus raathi* (NHMZ 2222), anterolateral view. **q**, Left femur, proximal end, *Saturnalia tupiniquim* (MCP 3844-PV), anterolateral view. Scale bars 1 cm. a., articulates with; at, anterior trochanter; bs, brevis shelf; dlt, dorsolateral trochanter; emg, external mandibular groove; g, glenoid; lia, linea intramuscularis cranialis; ol, olecranon process; sp, splenial; ts, trochanteric shelf.

Reporting Summary

Nature Portfolio wishes to improve the reproducibility of the work that we publish. This form provides structure for consistency and transparency in reporting. For further information on Nature Portfolio policies, see our [Editorial Policies](#) and the [Editorial Policy Checklist](#).

Statistics

For all statistical analyses, confirm that the following items are present in the figure legend, table legend, main text, or Methods section.

n/a Confirmed

- The exact sample size (n) for each experimental group/condition, given as a discrete number and unit of measurement
- A statement on whether measurements were taken from distinct samples or whether the same sample was measured repeatedly
- The statistical test(s) used AND whether they are one- or two-sided
Only common tests should be described solely by name; describe more complex techniques in the Methods section.
- A description of all covariates tested
- A description of any assumptions or corrections, such as tests of normality and adjustment for multiple comparisons
- A full description of the statistical parameters including central tendency (e.g. means) or other basic estimates (e.g. regression coefficient) AND variation (e.g. standard deviation) or associated estimates of uncertainty (e.g. confidence intervals)
- For null hypothesis testing, the test statistic (e.g. F , t , r) with confidence intervals, effect sizes, degrees of freedom and P value noted
Give P values as exact values whenever suitable.
- For Bayesian analysis, information on the choice of priors and Markov chain Monte Carlo settings
- For hierarchical and complex designs, identification of the appropriate level for tests and full reporting of outcomes
- Estimates of effect sizes (e.g. Cohen's d , Pearson's r), indicating how they were calculated

Our web collection on [statistics for biologists](#) contains articles on many of the points above.

Software and code

Policy information about [availability of computer code](#)

Data collection

Provide a description of all commercial, open source and custom code used to collect the data in this study, specifying the version used OR state that no software was used.

Data analysis

Beast 2, v. 2.6.3 for Bayesian phylogenetic inference; R statistical environment v. 4.2.0 with BioGeoBEARS package 1.1.2 for biogeographical analysis; TNT v. 1.5 for parsimony phylogenetic inference. All software and code is available on the online repository DRYAD (<https://doi.org/10.5061/dryad.pg4f4qrqd>)

For manuscripts utilizing custom algorithms or software that are central to the research but not yet described in published literature, software must be made available to editors and reviewers. We strongly encourage code deposition in a community repository (e.g. GitHub). See the Nature Portfolio [guidelines for submitting code & software](#) for further information.

Data

Policy information about [availability of data](#)

All manuscripts must include a [data availability statement](#). This statement should provide the following information, where applicable:

- Accession codes, unique identifiers, or web links for publicly available datasets
- A description of any restrictions on data availability
- For clinical datasets or third party data, please ensure that the statement adheres to our [policy](#)

All data files used for analyses are hosted on DRYAD (<https://doi.org/10.5061/dryad.pg4f4qrqd>). All fossils are reposed in recognized natural history institutions. To preserve the integrity of the fossil localities and the natural history resources of Zimbabwe, we do not present the geographic coordinate data here. Geographic coordinate data are available on request from the Natural History Museum of Zimbabwe (NHMZ), and are recorded in the specimen catalog and records of the NHMZ for full reproducibility.

Field-specific reporting

Please select the one below that is the best fit for your research. If you are not sure, read the appropriate sections before making your selection.

- Life sciences Behavioural & social sciences Ecological, evolutionary & environmental sciences

For a reference copy of the document with all sections, see nature.com/documents/nr-reporting-summary-flat.pdf

Ecological, evolutionary & environmental sciences study design

All studies must disclose on these points even when the disclosure is negative.

Study description	Recovery of fossilized material from the Triassic of Zimbabwe; placing material into a phylogeny of early dinosaurs and using this phylogeny to test hypothesis of biogeographic dispersal
Research sample	Fossils recovered from a single site in the Pebby Arkose Formation of northern Zimbabwe: a sauropodomorph (<i>Mbiresaurus raathi</i> , gen. et sp. nov.), a herrarasaurid, a hyperodapedontine rhynchosaur, a traversodontid cynodont, aetosaur
Sampling strategy	Standard palaeontological excavation methods
Data collection	Anatomical and histological observation
Timing and spatial scale	Fieldwork proceeded July–August 2017; May–June 2019
Data exclusions	NA
Reproducibility	All fossils reposed in recognized natural history museums
Randomization	NA
Blinding	NA

Did the study involve field work? Yes No

Field work, collection and transport

Field conditions	Dry season, warm, mild, no rainfall
Location	Dande Communal Area, Mbire District, Zimbabwe
Access & import/export	NA
Disturbance	NA

Reporting for specific materials, systems and methods

We require information from authors about some types of materials, experimental systems and methods used in many studies. Here, indicate whether each material, system or method listed is relevant to your study. If you are not sure if a list item applies to your research, read the appropriate section before selecting a response.

Materials & experimental systems

n/a	Involved in the study
<input checked="" type="checkbox"/>	Antibodies
<input checked="" type="checkbox"/>	Eukaryotic cell lines
<input type="checkbox"/>	Palaeontology and archaeology
<input checked="" type="checkbox"/>	Animals and other organisms
<input checked="" type="checkbox"/>	Human research participants
<input checked="" type="checkbox"/>	Clinical data
<input checked="" type="checkbox"/>	Dual use research of concern

Methods

n/a	Involved in the study
<input checked="" type="checkbox"/>	ChIP-seq
<input checked="" type="checkbox"/>	Flow cytometry
<input checked="" type="checkbox"/>	MRI-based neuroimaging

Palaeontology and Archaeology

Specimen provenance	Zimbabwe. All foreign researchers involved in fieldwork (C.T.G., S.T., S.J.N.) were registered with the Research Council of Zimbabwe for 2017 and 2019 field seasons (permit number 02991 and 03266 to C.T.G.; 02992 to S.T.; 03267 to S.J.N.).
Specimen deposition	Specimens deposited in Natural History Museum of Zimbabwe, Bulawayo, Zimbabwe
Dating methods	Detrital zircon dating was attempted, but the obtained age indicated that the processes that created these zircons occurred long before the deposition of our Carnian locality. Dating was therefore based primarily on biostratigraphy

Tick this box to confirm that the raw and calibrated dates are available in the paper or in Supplementary Information.

Ethics oversight All foreign researchers registered with the Research Council of Zimbabwe.

Note that full information on the approval of the study protocol must also be provided in the manuscript.